GEOLOGICA CARPATHICA, 2025, 76, 3, 209–224 https://doi.org/10.31577/GeolCarp.2025.14

Evolution of accessory Nb–Ta–W–Sn–Ti–Fe oxide minerals from the Markersbach highly evolved aluminous A-type granite, Erzgebirge, Germany: Magmatic to hydrothermal processes and elemental mobility during F-rich fluid–rock interaction

MARTIN ONDREJKA[1,✉], HANS-JÜRGEN FÖRSTER[2], MAËLYS BÉVAN[1], PAVEL UHER[1], CHRISFANEL EURODE KIANGUEBENE-KOUSSINGOUNINA[1] and NASSER M. MAHDY[3]

[1]Department of Mineralogy Petrology and Economic Geology, Faculty of Natural Sciences, Comenius University, Ilkovičova 6, Mlynská dolina, 842 15, Bratislava, Slovakia
[2]Helmholtz Centre Potsdam GFZ German Research Centre for Geosciences, D-14473 Potsdam, Germany
[3]Nuclear Materials Authority, P.O. 530, El-Maadi, Cairo, Egypt

(Manuscript received May 29, 2025; accepted in revised form August 25, 2025; Associate Editor: Milan Kohút)

Abstract: The Markersbach granite (Erzgebirge/Krušné Hory, Germany) is a late Variscan, post-collisional, highly evolved and autometasomatically altered, high-F and low-P aluminous A-type leucogranite. The diversity of Nb–Ta–W–Sn–Ti–Fe oxide minerals within the Markersbach granite was studied here by electron probe microanalysis to unveil the chemical evolution of the system during magmatic to hydrothermal stages. The rock-forming minerals of the granite comprise quartz, perthitic K-feldspar, albite, and Li-rich annite to Li-rich siderophyllite (zinnwaldite). Accessory minerals are zircon, thorite, and rarely monazite-(Ce), xenotime-(Y), and chernovite-(Y), topaz, fluorite, REE–Ca–Th fluorocarbonates and fluorides–oxyfluorides, and the Nb–Ta–W–Sn–Ti–Fe oxide phases. Common W-rich columbite supergroup minerals (nioboixiolite series, columbite-(Fe), qitianlingite) and minor Nb–Ta-rich rutile, cassiterite, minerals of the pyrochlore supergroup and Nb-rich ferric oxide (goethite?) were identified in the granite. Oscillatory-zoned nioboixiolite I, recrystallized patchy nioboixiolite II and columbite-(Fe) are rich in W (≤38.8 wt.% WO_3; ≤0.2 apfu W), while cassiterite and mainly rutile are rich in Nb and Ta (≤18.5 wt.% Nb_2O_5; ≤0.13 apfu Nb; ≤21.1 wt.% Ta_2O_5; ≤0.1 apfu Ta). Minerals of the pyrochlore supergroup commonly replace columbite supergroup minerals and show a wide compositional variability for U, Th, REE, Pb, W and Si. At the scale of individual minerals, the evolution of the Mn/(Fe+Mn) and Ta/(Nb+Ta) ratios differs and reflects complex fluid–melt interactions. These compositional variations and textural observations suggest the late-magmatic crystallization of oscillatory zoned nioboixiolite I and small disseminated, compositionally homogenous, columbite-(Fe). The marginal domains of nioboixiolite II, Nb–Ta rich porous cassiterite, rutile and qitianlingite replacing columbite-(Fe) are probably of late-magmatic to early post-magmatic origin. This late evolution reflects a F-rich character of the system, evolving from a melt-dominated to a more fluid-driven regime, under flux-rich magmatic conditions. Lower temperature fluids induced the partial dissolution and in-situ metasomatic replacement of primary ore minerals combined with a minor remobilization of rare metals, giving rise to pyrochlore supergroup minerals and Nb-rich goethite-like mineral. This ferric oxide represents the latest rare-metal bearing phase in the Markersbach granite, as well as a unique secondary host of, geochemically less mobile, Nb.

Keywords: nioboixiolite, Nb-Ta minerals, A-type granite, Markersbach, Erzgebirge

Introduction

Highly evolved, late- to post-orogenic aluminous (leuco)granites and granitic pegmatites may be enriched in key granitophile rare lithophile elements, such as Li, Rb, Cs, Be, Sn, Nb, Ta, and W. The concentration of these elements could be several orders of magnitude above their respective crustal values (Taylor & McLennan 1985; Černý et al. 2005). These highly fractionated granitic rocks containing anomalous concentrations of these elements are often referred to as rare metal granites/pegmatites. Mineralization of Nb, Ta, Sn, and W are usually developed in the proximity of these granite intrusions and show a notable genetic diversity, ranging from pluton-hosted breccia and hydrothermal vein-stockwork systems to (peri)batholitic greisens, skarns, pegmatites, and hydrothermal veins (e.g., Hulsbosch 2019; Romer & Pichavant 2021). Peraluminous rare-metal granites with magmatic disseminated Nb, Ta, Sn and W mineralization are locally associated with vein- and greisen-type mineralization (Breiter et al. 1999), the origin of both requiring fluid saturation under

✉ corresponding author: Martin Ondrejka
martin.ondrejka@uniba.sk

hydrostatic conditions (Černý et al. 2005). A wide range of high-field-strength element (HFSE; Sn, Nb, Ta, W) and other rare metal-bearing accessory minerals have been described from the Variscan Erzgebirge (Krušné Hory) granite-related metallogenetic province, situated on both sides of the Czech–German border. These accessory phases include Nb–Ta–Ti–Sn–W oxides, uraninite, monazite-(Ce), xenotime-(Y), zircon, thorite, REE–Ca–Th fluorocarbonates and fluorides–oxyfluorides. These minerals reflect the complex compositions of the parental granites, manifest their interactions with F- and CO_2-rich fluids and have been widely used for description and interpretation of the evolution of fractionated magmatic systems (e.g., Johan & Johan 1994; Förster 1998a, 1998b, 1999, 2006; Förster et al. 2011; Breiter et al. 2016, 2017).

In this work, we studied a complex Nb–Ta–W–Sn–Ti–Fe accessory mineral assemblage from the Markersbach granite pluton, Erzgebirge, Germany (Fig. 1). Its mineralogy, and in particular its accessory minerals content and associated chemistry, is still not yet sufficiently well constrained. The aim of this work was to thoroughly study the textural–compositional characteristics of these mineral species, to highlight their evolution from the magmatic to the hydrothermal stage. In addition, identification of unusual mineral species prompted a detailed crystal-chemistry study, to determine associated compositional variations and relevant substitution mechanisms. Special attention was directed to the role of dissolution–reprecipitation processes that occurred under conditions of F-rich fluid–rock interaction and facilitated the remobilization of Nb and Ta, elements usually considered immobile. The study of other accessory and secondary minerals, namely those bearing REE, Th, U, Zr, Hf, and F, is beyond the scope of this article and will be the subject of a forthcoming paper.

Geological and geochemical background

The Variscan Erzgebirge (Krušné Hory) mountain range is positioned in the border region between Germany (Saxony) and the Czech Republic, at the northwestern margin of the Bohemian Massif. It represents a NE–SW-trending antiformal structure in the Saxothuringian Zone of the Variscan orogen. The Erzgebirge exposes crystalline basement rocks of Proterozoic and Paleozoic protolith ages which were metamorphosed in the early Carboniferous in response to crustal thickening in result of the Variscan continental collision (e.g., Mingram 1998; and references therein). Shortly after orogenic collapse and subsequent crustal thinning, in the late Carboniferous and early Permian, large masses of granitic rocks, rhyodacitic–rhyolitic lava flows and lamprophyric dykes were emplaced during multiple events. The granites typically form multiphase plutons of various sizes and compositions that are of late- to post-collisional origin. The Erzgebirge is

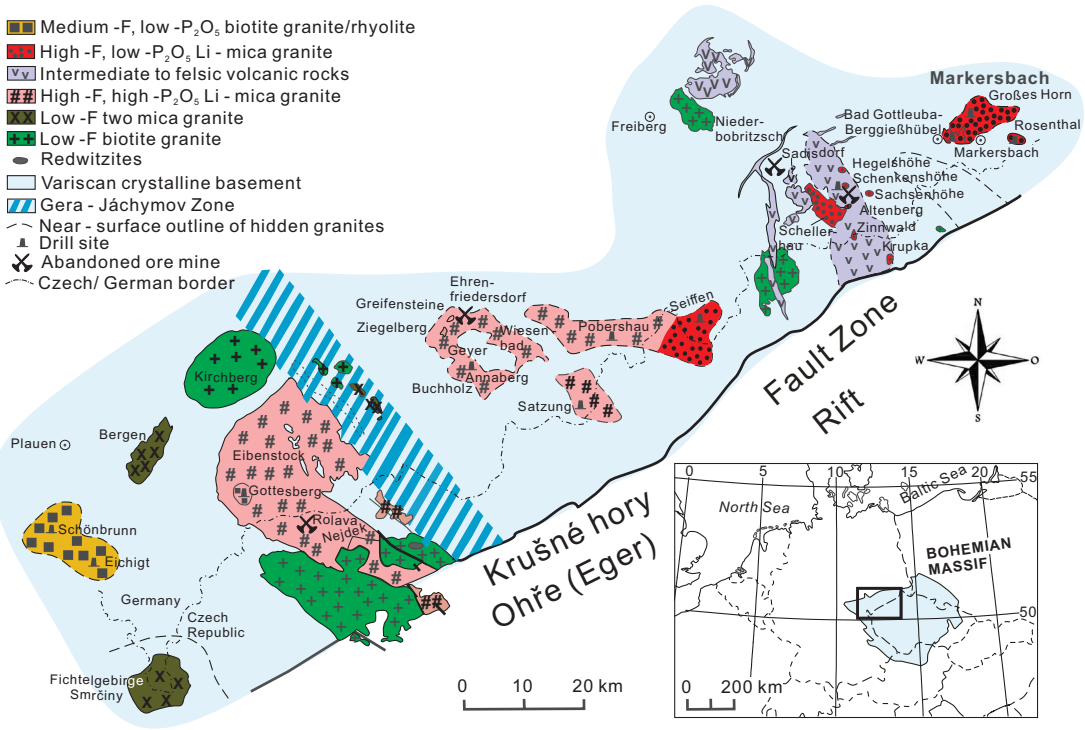

Fig. 1. Simplified geological sketch-map showing the occurrences and regional distribution of the various types of Variscan granites in the Erzgebirge–Vogtland metallogenetic province and the geographical position of the Markersbach granite. The bulk of granites in the west and east are outcropping whereas those in the central part are mostly known from drilling and ore mining. The surface samples (1042, 1044, 1046 and 1047) are collected at Großes Horn elevation (GPS: 50°51'35.0"N 13°57'40.5"E) 1.8 km NW of Bad Gottleuba–Berggießhübel and the drillhole, near-surface sample 1096 (depth 116 m, GPS: 50°50'42.3"N 13°58'56.3"E) is 0.7 km N of Markersbach (modified from Förster et al. 1999).

particularly well known for the widespread occurrence of compositionally evolved granites (Fig. 1) spatially and genetically associated which magmatic Sn–W and post-magmatic U deposits.

According to mineralogical, geochemical, isotopic, and age criteria, the Variscan Erzgebirge granites are subdivided into five major groups (Förster et al. 1999): (1) low-F biotite granites; (2) low-F two-mica granites; (3) high-F, high-P Li-mica granites; (4) high-F, low-P Li-mica granites, and (5) moderate-F, low-P biotite granites. Granites of groups 1–3 are late-collisional, and they are classified as transitional between I- and S-type (groups 1 and 2) to S-type (group 3). Granites of group 4 are late-collisional, whereas those of group 5 are post-collisional. Both display compositional features of aluminous A-type rocks and highly fractionated I-type granites in the sense of Chappell (1999). The granite referred to in this paper is representative of group 4.

The Markersbach granite is located in the easternmost Erzgebirge in Germany, at the transition to the Elbe Zone and spatially associated with the Cretaceous Königshain uranium deposit located in Upper Cretaceous sandstones. About 5 km^2 of the granite body is exposed at the present surface. Drilling and mining activities in connection with the search for U deposits provided additional underground exposures of the granite down to several 100 meters. According to texture and grain size, at least three lithotypes could be distinguished. It is yet unknown whether these lithotypes formed during a single event or represent different pulses of magma emplacement. Inadequate information also exists with respect to the erosion level of the pluton, but it is fair to assume that the present surface does not represent the former apical part built up of more evolved and syn- to post-magmatically overprinted granite portions still more enriched in LILE and HFSE elements. At the present levels of exposure, neither zones of greisenization nor ore-bearing veins were observed.

The Markersbach granite represents a highly evolved aluminous leucogranite of A-type affinity. Its A/CNK ratio ranges from 0.96 to 1.05 and corresponds to a metaluminous to slightly peraluminous character (Förster 2001). Its evolved nature is evidenced by very low contents of Ca (0.15–0.60 wt.% CaO), Mg (0.01–0.04 wt.% MgO), Sr (0.8–5.7 ppm), Ba (8–20 ppm), and extremely low P (0.007–0.02 wt.% P_2O_5), combined with low Zr/Hf (11.6–16.6), Nb/Ta (3.8–8.6) and K/Rb (≤100) ratios. The impact of late- to post-magmatic overprinting is not restricted to components that are relatively easy to mobilize, such as Ca, Na (3.2–4.4 wt.% Na_2O), F (2100–8300 ppm), Li (27–450 ppm), Rb (421–1000 ppm), and Cs (5.9–33 ppm), but is observed also for elements that are normally considered less mobile; Th (33–60 ppm), the LREE (81–153 ppm), Y (55–136 ppm), and the other HREE (41–75 ppm). The concentrations of the rare metals Sn (5–26 ppm), W (6–14 ppm), Mo (<0.2–3.7 ppm), Nb (31–55 ppm), and Ta (4.2–11.3 ppm) are equally variable. The observed large variations in elemental concentrations cannot be explained only in terms of simple crystal fractionation and differentiation but involves a significant elemental redistribution during fluid–rock interaction (Förster 2001; Štemprok et al. 2003). The initial magmatic concentrations of most of the LILE, HFSE and rare metals were probably at the upper end of their observed range, i.e., alteration-induced elemental redistribution gave rise to their depletion.

Analytical methods

The chemical composition of accessory minerals was studied using a JEOL JXA-8530F electron probe microanalyzer (EPMA) working in the wavelength-dispersive spectrometry (WDS) mode at the Earth Science Institute, Slovak Academy of Sciences, Banská Bystrica, Slovakia. An accelerating voltage of 15 kV and a probe current of 20 nA were applied. The beam (spot) diameter varied from 2 to 6 μm; a more focused ≤1–3 μm beam was used only occasionally, to avoid "mixed" analyses in areas characterized by a strongly heterogeneous composition at the microscale. Materials used as calibration standards involved natural minerals and synthetic substances (Table 1), and raw counts were converted to wt.% of oxides using the ZAF matrix correction. Corrections of line interferences were provided using the method by Åmli & Griffin (1975). The detection limit for all elements is typically between 0.01 and 0.15 wt.%.

A selection of accessory minerals was additionally measured using a Cameca SX100 microanalyzer at the Department of Electron Microanalysis at the State Geological Institute of Dionýz Štúr, Bratislava, Slovakia, as well operating in wavelength dispersive mode. An accelerating voltage of 15 kV and a probe current of 20–35 nA were used; other relevant analytical conditions were selected according to mineral type, i.e., whether the phase is highly or poorly resistant to destruction under the electron beam. The typical beam diameter varied from 3 to 5 μm. The EPMA was calibrated using natural and synthetic standards (Table 1), and raw counts were converted to oxide wt.% using 'PAP' matrix correction factors (Pouchou & Pichoir 1985). Notably, measurements performed under differing analytical conditions and different elemental standards (Table 1) gave consistent results within the limits of error.

Lithium in micas was estimated from Si content using empirical equation Li_2O (wt.%)=[0.289*SiO_2(wt.%)]−9.658 (Tischendorf et al. 1997). Element contents in the mineral formulae are expressed in atoms per formula unit (apfu). The cassiterite, rutile, nioboixiolite formulae were normalized to 2 oxygen atoms, and qitianlingite to 10 oxygen atoms. The formulae of columbite group species were normalized on 6 oxygen atoms; their naming considered the nomenclature, classification (Chukanov et al. 2023), and formulae extended Levinson suffix revision published by Bosi et al. (2024) and Chukanov et al. in press). The root name "nioboixiolite" with no suffix refers to ferrous-ferric Nb-dominant ixiolite series, while "wolframoixiolite" refers to mineral composition similar to that described by Ginzburg et al. (1969). The concentrations of Fe^{2+} and Fe^{3+} in the studied Nb–T–Sn–W–Ti–Fe oxide minerals were calculated from ideal stoichiometry based on

Table 1: Analytical conditions used for the electron microprobe analyses.

EPMA in Bratislava				detect. limit (3σ)	EPMA in Banská Bystrica				detect. limit (3σ)
element	line	crystal	standard	in ppm	element	line	crystal	standard	in ppm
W	*La*	LLIF	$CaWO_4$	1235–1890	W	*La*	LIFL	scheelite	680–930
P	*Ka*	LPET	apatite	85–145	P	*Ka*	PETL	apatite	175–200
Nb	*La*	LPET	$LiNbO_3$	565–695	Nb	*La*	PETL	$LiNbO_3$	210–270
Ta	*La*	LLIF	$LiTaO_3$	760–2400	Ta	*Ma*	PETL	$CrTa_2O_6$	370–550
Si	*Ka*	TAP	wollastonite	150–385	Si	*Ka*	TAP	albite	65–230
Ti	*Ka*	LLIF	TiO_2	210–330	Ti	*Ka*	LIF	rutile	360–555
Zr	*La*	LPET	$ZrSiO_4$	465–1130	Zr	*La*	PETH	cubic zirconia	130–205
Hf	*La*	LLIF	HfO_2	1100–1200	Hf	–	–	–	–
Sn	*La*	LPET	SnO_2	305–415	Sn	*La*	PETL	cassiterite	150–190
Th	*Ma*	LPET	ThO_2	365–390	Th	*Ma*	PETL	thorianite	220–250
U	*Mb*	PET	UO_2	615–1095	U	*Mb*	PETL	UO_2	275–485
Al	*Ka*	TAP	Al_2O_3	140–225	Al	–	–	–	–
Sc	*Ka*	LLIF	$ScPO_4$	195–405	Sc	*Ka*	LIF	$ScVO_4$	255–410
Y	*La*	LPET	YPO_4	435–635	Y	*La*	PETL	YPO_4	220–265
La	*La*	LLIF	$LaPO_4$	790–825	La	*La*	LIFH	$LaPO_4$	365–430
Ce	*La*	LLIF	$CePO_4$	685–775	Ce	*La*	LIFH	$CePO_4$	300–365
Pr	*Lb*	LLIF	$PrPO_4$	725–780	Pr	*Lb*	LIFH	$PrPO_4$	605–715
Nd	*La*	LLIF	$NdPO_4$	590–660	Nd	*La*	LIFH	$NdPO_4$	500–565
Sm	*La*	LLIF	$SmPO_4$	720–830	Sm	*Lb*	LIFH	$SmPO_4$	285–340
Eu	*Lb*	LLIF	$EuPO_4$	850–950	Eu	–	–	–	–
Gd	*La*	LLIF	$GdPO_4$	760–825	Gd	*Lb*	LIFH	$GdPO_4$	650–685
Tb	*La*	LLIF	$TbPO_4$	1150–1275	Tb	–	–	–	–
Dy	*Lb*	LLIF	$DyPO_4$	1115–1235	Dy	–	–	–	–
Ho	*Lb*	LLIF	$HoPO_4$	1270–1315	Ho	–	–	–	–
Er	*Lb*	LLIF	$ErPO_4$	1300–1430	Er	–	–	–	–
Tm	*La*	LLIF	$TmPO_4$	1030–1140	Tm	–	–	–	–
Yb	*La*	LLIF	$YbPO_4$	930–995	Yb	–	–	–	–
Lu	*Lb*	LLIF	$LuPO_4$	2050–2225	Lu	–	–	–	–
Sb	–	–	–	–	Sb	*La*	PETH	stibnite	195–200
Fe	*Ka*	LLIF	fayalite	305–765	Fe	*Ka*	LIF	hematite	260–375
Ca	*Ka*	LPET	wollastonite, apatite	120–185	Ca	*Ka*	PETH	diopside, apatite	45–125
Pb	*Ma*	LPET	$PbCO_3$	570–655	Pb	–	–	–	–
Ba	*La*	LPET	baryte	310–360	Ba	*La*	LIF	baryte	1305–2135
Mn	*Ka*	LLIF	rhodonite	280–730	Mn	*Ka*	LIF	rhodonite	320–400
Zn	*Ka*	LLIF	willemite	715–820	Zn	*Ka*	LIF	gahnite	690–800
Mg	*Ka*	TAP	MgO, forsterite	165–240	Mg	*Ka*	TAP	pyrope	100–115
Na	*Ka*	TAP	albite	300–360	Na	*Ka*	TAP	albite	110–260
K	*Ka*	LPET	orthoclase	180–195	K	–	–	–	–
F	*Ka*	LPC0	CaF_2	300–350	F	*Ka*	LDE1	fluorite	625–730
Cl	*Ka*	LPET	NaCl	160–200	Cl	*Ka*	PETL	tugtupite	50–65

cations and neutral charge balance. The formula proportions of the pyrochlore supergroup minerals were normalized to 2 cations on *B* site, adopting the nomenclature of Atencio et al. (2010). All mineral compositional plots were constructed using the CorelKit plug-in for CorelDRAW (Zhang et al. 2023).

Results

Petrography and mineralogy of the Markersbach granites

The studied granite samples show a diversity in terms of texture and mineralogy. One lithotype is a pink-red, porphyritic to glomerophyric fine-grained syenogranite with varying phenocryst–matrix ratios, frequently displaying granophyric to (micro-)graphic textures. The second lithotype is a greyish, porphyritic to glomerophyric fine-grained monzogranite. Finally, the third type is a medium- to coarse-grained monzogranite. All lithotypes show a low intensity of ductile deformation, with undulose extinction and sporadic deformation lamellae in quartz, while feldspar displays a discreet (lithotype 1 and 2) to moderate (lithotype 3) formation of subgrains by bulging recrystallization. Typical magmatic mineralogy consists of quartz, anhedral to subhedral perthitic K-feldspar ($Or_{98–76}Ab_{24–2}An_0$) to antiperthitic–mesoperthitic alkali feldspar ($Or_{30–19}Ab_{80–70}An_0$), euhedral to subhedral albitic plagioclase ($Ab_{95–98}An_{0–2}Or_{1–5}$), and late euhedral albite. Trioctahedral micas are widespread. Magmatic, euhedral dark brown crystals occur sporadically. More abundant are late-magmatic to

postmagmatic–hydrothermal pale green subhedral crystals, which commonly exhibit internal zonation. They have Li-bearing siderophyllite–annite cores and Li-rich siderophyllite (zinnwaldite) rims with calculated Li content ≤2.3 wt.% Li_2O (≤0.7 apfu Li). The contents of Fe and Mn vary from 18.8 to 28.9 wt.% FeO_{total} and from 0.5 to 0.9 wt.% MnO, respectively with Mn/(Mn+Fe)=0.02 to 0.03 apfu. Fluorine content is relatively high (≤7.0 wt.%) which corresponds to a markedly dominant (F,Cl,OH)-site occupancy (≤1.65 apfu). Fresh trioctahedral micas commonly bear hematite and rarely also Nb-free rutile and ilmenite/magnetite. Dioctahedral micas are represented by muscovite exhibiting significantly lower Li and F contents in comparison to trioctahedral micas (≤1.0 wt.% Li_2O; 0.25 apfu Li, and ≤2.0 wt.% F; 0.4 apfu).

Mineralogical and textural evidence of hydrothermal alteration include minor sericitization of plagioclase and chloritization of Li-rich siderophyllite occurred locally. Late-magmatic(?) and hydrothermal fluorite is a typical constituent of the Markersbach granite, with Ca supplied during destabilization of plagioclase and F released during breakdown of the micas. Rare late-magmatic topaz I, which generally occurs as inclusions in quartz and plagioclase, predates the formation of metasomatic topaz II, interstitial between late quartz and albite. Other accessory minerals comprise abundant Nb–Ta–W–Sn–Ti–Fe oxides (columbite supergroup minerals, rutile, cassiterite and pyrochlore supergroup minerals), zircon, thorite, and rarely monazite-(Ce), xenotime-(Y), and chernovite-(Y). Many of the Zr–Th–U–Y–REE minerals represent a complex thorite–coffinite–zircon–xenotime solid solutions. Rare accessory monazite-(Ce) and xenotime-(Y) are the only phosphates occurring in the Markersbach granite.

Nb–Ta–Sn–W–Ti–Fe oxide minerals

Minerals containing Nb, Ta, Sn W, Fe and Ti as major constituents are abundant accessory phases in the Markersbach granite (Fig. 2a). They are represented by cassiterite, Nb–Ta-rich rutile, nioboixiolite-(Fe^{3+}), "nioboixiolite-(Fe^{2+})" a qitianlingite-like phase (Table 2), columbite-(Fe) (Table 3), pyrochlore supergroup minerals and Nb-rich ferric oxides (goethite?) (Table 4).

Cassiterite occurs rarely as scattered and solitary crystals. It also forms subhedral porous crystals (~50 to 100 μm in size). Cassiterite usually crystallized in close association with columbite supergroup minerals, locally overgrowing nioboixiolite I and intergrowing with nioboixiolite II in fluorite and feldspars (Fig. 2b). It is enriched in Nb (≤5.0 wt.% Nb_2O_5; 0.06 apfu Nb) and Ta (2.7 wt.% Ta_2O_5; 0.02 apfu Ta); the Ta/(Nb+Ta) ratio varies between 0.24 and 0.51 (Fig. 3). Some cassiterite crystals are enriched in Ti and Fe (≤1.1 wt.% TiO_2; 0.02 apfu Ti and ≤2.7 wt.% FeO; 0.05 apfu Fe); the Mn/(Mn+Fe) ratio is very low (≤0.05) (Fig. 3, Table 2). The Fe content shows a positive correlation with the (Nb+Ta) content (Fig. 4a), implying the occurrence of the columbite- and/or ixiolite-type substitution mechanisms $(Fe,Mn)^{2+}+2(Nb,Ta)^{5+} \leftrightarrow 3Sn^{4+}$ and $Fe^{3+}+(Nb,Ta)^{5+} \leftrightarrow 2Sn^{4+}$ (Figs. 4b, 5). The concentration of Sc (≤0.11 wt.% Sc_2O_3, ≤0.002 apfu) is usually close to the detection limit of the electron microprobe.

Rutile is rare, only observed in close association with larger crystal aggregates composed of columbite supergroup minerals and cassiterite. It forms small (≤50 μm in size), subhedral satellite crystals (Fig. 2a–c), displaying a large compositional inhomogeneity of individual crystals, with apparent oscillatory and patchy secondary zoning (Fig. 2c). It is variably rich in Nb (6.7–18.5 wt.% Nb_2O_5; ≤0.13 apfu Nb) and Ta (1.6–21.1 wt.% Ta_2O_5; ≤0.1 apfu Ta); the atomic Ta/(Nb+Ta) and Mn/(Mn+Fe) ratios attain 0.05–0.49 and ≤0.01, respectively (Fig. 3, Table 2). Elevated Fe concentrations (10.8 wt.% FeO_{tot}; ≤0.16 apfu) positively correlate with the (Nb+Ta) content (Fig. 4a), pointing to the columbite and/or ixiolite-type substitution mechanisms $(Fe,Mn)^{2+}+2(Nb,Ta)^{5+} \leftrightarrow 3Ti^{4+}$ and $Fe^{3+}+(Nb,Ta)^{5+} \leftrightarrow 2Ti^{4+}$ (Figs. 4b, 5). Rutile reveals increased contents of W, especially at the rim (≤1.5 wt.% WO_3), and Sn (≤1.4 wt.% SnO_2), the amount of Sc attains up to 0.13 wt.% Sc_2O_3 (Table 2).

A complex Nb–Ta–W–Fe-rich phase, which has a stoichiometry very close to W-rich nioboixiolite series (ixiolite group), occurs frequently in the Markersbach granite. It crystallized as large, euhedral and oscillatory zoned crystals (≤250 μm in size) preferentially in alkali feldspars, albite, and fluorite, where it is intimately associated with cassiterite and rutile. The oscillatory zoned domains (nioboixiolite I) mainly reflect Nb–Ta–W variations (Fig. 2b). The marginal parts contain domains with truncated, irregular boundaries and patchy secondary zoning (Fig. 2b), documenting Nb–W variations, while Ta content is nearly constant. These recrystallized domains (nioboixiolite II) stoichiometrically fit to "wolframoixiolite" and represent an intermediate composition along the columbite-(Fe)–ferberite join (Fig. 5). The central parts of these large crystal aggregates are darker in BSE and represent the transformation into altered and porous mixture of nioboixiolite series (Fig. 2b, d) and Nb–Ta-rich hydrous, ferric oxide–hydroxide (possibly goethite?) (Fig. 2d) with ≤13.7 wt.% Nb_2O_5 and 6.9 wt.% Ta_2O_5 (Table 4). The specific compositional signature of the nioboixiolite series is the significant enrichment of W omnipresent in all studied samples (9.1–38.8 wt.% WO_3; ≤0.2 apfu W). Further, it contains 24.7–55.3 wt.% Nb_2O_5 (≤0.4 apfu Nb), 16.3–23.5 wt.% FeO_{tot} (≤0.4 apfu Fe_{tot}), and 3.4–23.6 wt.% Ta_2O_5 (0.15 apfu Ta), as well as elevated contents of Mn, Ti, and Sc. The Ta/(Nb+Ta) and Mn/(Mn+Fe) ratios attain 0.06–0.34 and 0.05–0.21, respectively (Fig. 3, Table 2). Considering the Nb>W and M^{3+} : M^{2+} cation relationships as well as the assumption of a disordered cation distribution, the corresponding end-members are nioboixiolite-(Fe^{3+}) $(Nb_{0.5}Fe^{3+}_{0.5})O_2$, with $M^{3+}>M^{2+}$, and Fe^{2+}-dominant nioboixiolite ["nioboixiolite-(Fe^{2+})"] $(Nb_{0.67}Fe^{2+}_{0.33})O_2$, with $M^{2+}>M^{3+}$, the latter mineral not yet approved as valid IMA-CNMNC mineral (Table 2).

Columbite-(Fe) is the only identified species of the columbite group. It occurs as small, disseminated crystals (≤20 μm) in quartz (Fig. 2e) and as individual crystals (≤80 μm in size) scattered in micas, quartz, or feldspars. The larger crystals

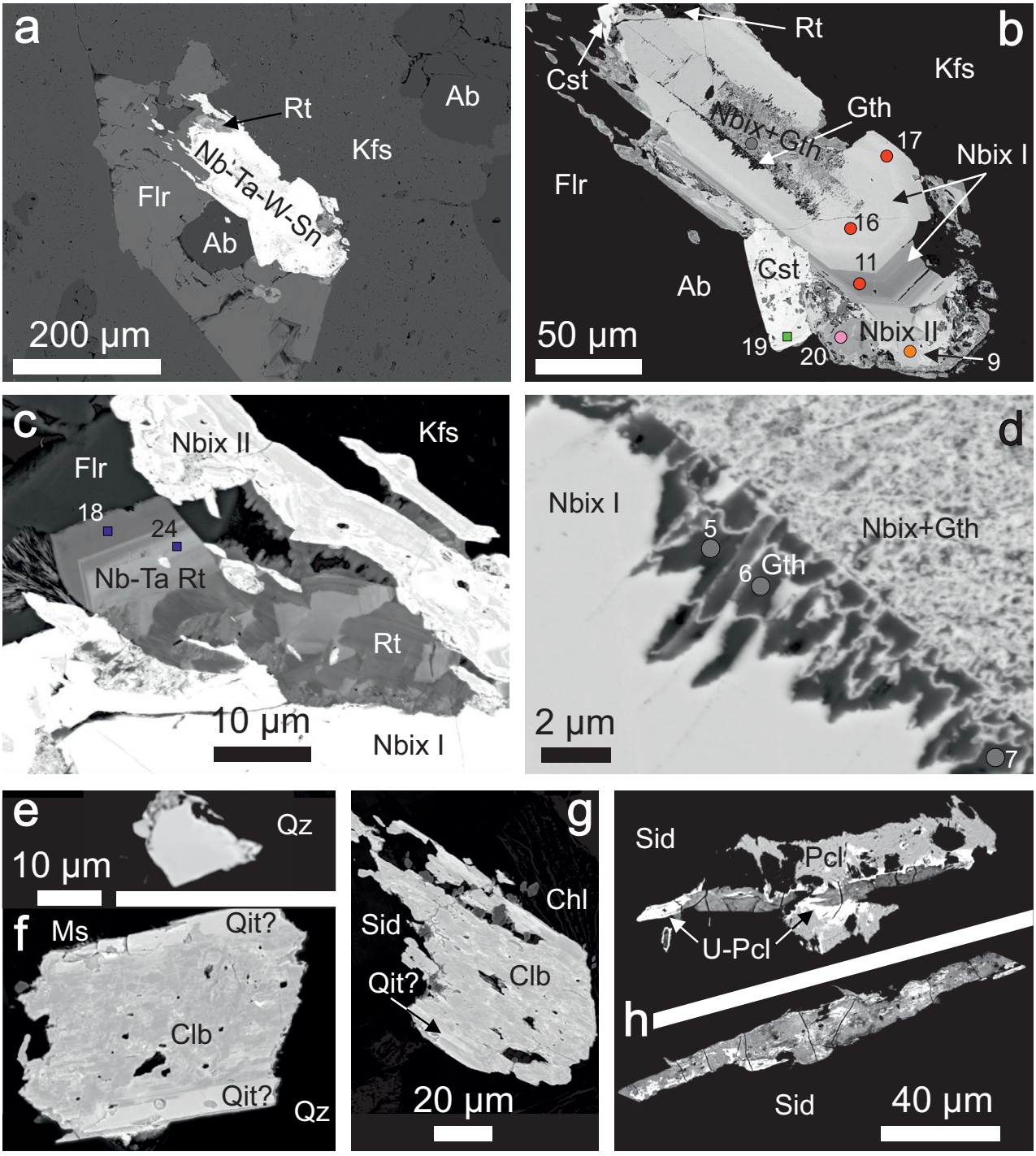

Fig. 2. Back-scattered electron images of primary and secondary Nb–Ta–W–Sn–Ti–Fe accessory minerals in the Markersbach granite: **a** — the aggregate of Nb–Ta–W–Sn minerals and rutile (Rt) in association with K-feldspar (Kfs), albite (Ab) and fluorite (Flr); **b** — an aggregate (a) of large oscillatory zoned nioboixiolite (Nbix I) with marginal domains of nioboixiolite II (Nbix II). The central part represents an alteration-induced mixture of nioboixiolite–ferric oxide (possibly goethite) (Nbix, Gth). The associated minerals within the aggregate are rutile (Rt) and porous cassiterite (Cst).; **c** — a detailed view of Nb+Ta-rich rutile (Nb–Ta Rt) situated in the large crystal aggregate of nioboixiolite (Nbix) shown in (b). Other minerals are K-feldspar (Kfs) and fluorite (Flr); **d** — a detailed view of the transitional domain between nioboixiolite I (Nbix I) and the altered central part of nioboixiolite–ferric oxide (possibly goethite) mixture (Nbix, Gth). The lobate infiltrations, dark in BSE, are ferric oxide, most probably goethite (Gth) with elevated content of Nb; **e** — disseminated tiny crystal of compositionally homogeneous columbite-(Fe) in quartz; **f, g** — subhedral–anhedral crystals of columbite-(Fe) with secondary patchy zoning (Clb) and marginal qitianlingite-like phase (Qit?) in muscovite (Ms) and siderophyllite (Sid)–chlorite (Chl); **h** — irregular and heterogeneous, elongated pyrochlore aggregates (Pcl) in siderophyllite (Sid). White zones are U-rich (U-Pcl). IMA–CNMNC approved mineral symbols according to Warr (2021). Coloured symbols are the same as in compositional diagrams and correspond to different mineral compositions and generations. Numbers refer to spot analyses in Tables 2 and 4.

Table 2: Representative results of EPMA analyses and calculated mineral formulae of cassiterite (Cst), rutile (Rt), nioboixiolite-(Fe^{3+}), "nioboixiolite-(Fe^{2+})" (Nbix) and qitianlingite (Qit). Note: n.a. – not analyzed; *=recalculated.

sample	1096	1096	1096	1096	1096	1096	1096	1096	1096	1096	1096	1096	1046
spot in Fig. 2		19		18	24		11	16	17		9	20	
mineral	Cst	Cst	Cst	Rt	Rt	Rt	Nbix I	Nbix I	Nbix I	Nbix I	Nbix II	Nbix II	Qit
WO_3 (wt.%)	0.00	0.00	0.00	1.54	0.50	0.58	15.28	21.82	15.80	13.77	21.27	18.09	34.65
Nb_2O_5	0.97	5.00	2.00	18.53	13.72	14.32	43.09	29.13	27.90	31.41	46.39	38.11	37.22
Ta_2O_5	1.65	2.66	1.13	1.63	21.05	13.91	5.39	16.32	23.28	20.80	6.66	9.78	4.44
TiO_2	0.23	1.14	0.88	66.99	53.44	60.41	5.43	1.07	1.83	3.25	2.24	2.72	0.98
ZrO_2	n.a.	n.a.	n.a.	0.00	0.00	0.00	0.54	0.75	0.62	0.21	n.a.	n.a.	0.15
SnO_2	96.96	88.44	95.69	1.19	0.72	1.10	5.20	5.89	7.15	5.77	0.54	5.07	0.48
Sc_2O_3	0.00	0.00	0.00	0.13	0.06	0.01	0.86	1.00	0.99	0.50	0.59	0.57	0.45
Y_2O_3	n.a.	n.a.	n.a.	0.03	0.00	0.03	0.00	0.05	0.00	0.00	n.a.	n.a.	0.00
Sb_2O_3	0.03	0.06	0.06	n.a.	n.a.	n.a.	n.a.	n.a.	n.a.	n.a.	n.a.	n.a.	n.a.
Fe_2O_3*	1.03	2.36	0.00	8.68	8.60	8.66	14.53	12.68	12.45	13.99	1.62	15.99	0.34
FeO*	0.00	0.53	1.07	1.67	3.32	2.30	9.09	9.73	8.67	8.52	14.81	8.36	18.11
MnO	0.01	0.02	0.05	0.07	0.07	0.10	1.09	1.25	1.30	1.02	4.28	1.47	2.98
CaO	0.15	0.00	0.09	0.00	0.00	0.00	0.05	0.04	0.06	0.02	0.00	0.11	0.01
ZnO	0.06	0.14	0.00	0.00	0.00	0.00	0.02	0.00	0.05	0.00	0.01	0.00	0.00
MgO	0.04	0.02	0.00	0.02	0.00	0.00	0.00	0.00	0.00	0.00	0.02	0.00	0.00
Total	101.13	100.37	100.97	100.48	101.48	101.41	100.57	99.73	100.10	99.26	98.42	100.27	99.81
W^{6+} (apfu)	0.000	0.000	0.000	0.006	0.002	0.002	0.081	0.128	0.093	0.080	0.116	0.101	0.970
Nb^{5+}	0.011	0.055	0.022	0.126	0.103	0.102	0.399	0.299	0.287	0.319	0.440	0.370	1.818
Ta^{5+}	0.011	0.018	0.008	0.007	0.095	0.060	0.028	0.101	0.144	0.127	0.038	0.057	0.130
Ti^{4+}	0.004	0.021	0.016	0.757	0.667	0.719	0.084	0.018	0.031	0.055	0.035	0.044	0.080
Zr^{4+}	–	–	–	0.000	0.000	0.000	0.005	0.008	0.007	0.000	–	–	0.008
Sn^{4+}	0.955	0.859	0.934	0.007	0.005	0.007	0.042	0.053	0.065	0.052	0.004	0.043	0.021
Sc^{3+}	0.000	0.000	0.000	0.002	0.001	0.000	0.015	0.020	0.020	0.010	0.011	0.011	0.042
Y^{3+}	–	–	–	0.000	0.000	0.000	0.000	0.001	0.000	0.000	–	–	0.000
Sb^{3+}	0.000	0.001	0.001	–	–	–	–	–	–	–	–	–	–
Fe^{3+}*	0.019	0.043	0.028	0.090	0.097	0.100	0.212	0.206	0.202	0.223	0.025	0.243	0.028
Fe^{2+}*	0.000	0.011	0.000	0.023	0.049	0.030	0.147	0.175	0.157	0.151	0.258	0.141	1.635
Mn^{2+}	0.000	0.000	0.001	0.001	0.001	0.001	0.019	0.024	0.025	0.019	0.076	0.027	0.273
Ca^{2+}	0.004	0.000	0.002	0.000	0.000	0.000	0.001	0.001	0.001	0.000	0.000	0.003	0.001
Zn^{2+}	0.001	0.002	0.000	0.000	0.000	0.000	0.000	0.000	0.001	0.000	0.000	0.000	0.000
Mg^{2+}	0.001	0.001	0.000	0.000	0.000	0.000	0.000	0.000	0.000	0.000	0.001	0.000	0.000
Total	1.006	1.011	1.012	1.019	1.020	1.021	1.033	1.034	1.033	1.036	1.004	1.040	5.006
Mn/(Mn+Fe)	0.00	0.01	0.01	0.01	0.01	0.01	0.05	0.06	0.07	0.05	0.21	0.07	0.14
Ta/(Nb+Ta)	0.50	0.25	0.27	0.05	0.48	0.37	0.07	0.25	0.33	0.28	0.08	0.13	0.07

typically exhibit complex patchy or irregular zoning (Fig. 2f, g), reflecting mainly fluctuations in Nb/W values. Abundant small crystals (≤20 μm) are compositionally homogeneous and exhibit the lowest Ta/(Nb+Ta) values. Generally, Ta/(Nb+Ta) values range between 0.01 to 0.09 and Mn/(Mn+Fe)=0.10–0.25 (Fig. 3). Commonly elevated contents of W, Ti, Sn, and Sc (Table 3) infer a relatively high structural disorder. However, the atomic (Nb+Ta)/(Fe+Mn) ratio is between 1.6–2.2, which is close to the value (~2.0) characteristic for the columbite group minerals. Columbite-(Fe) from Markersbach usually shows the limited content of the euxenite molecule ($YTiNbO_6$) with ≤2.1 wt.% REE_2O_3. Some spot analyses conducted in the brightest BSE domains (Fig. 2f, g) match the composition and stoichiometry of $Fe^{2+}{}_2Nb_2W^{6+}O_{10}$, suggesting the possible presence of qitianlingite (Table 2, Fig. 5).

Minerals of the pyrochlore supergroup and associated U–Nb–Ta phase form irregular slender, needle-like and elongated, locally porous aggregates (≤200 μm in size) in fluorite, feldspars and micas, frequently with desiccation cracks (Fig. 2h). The pyrochlore supergroup minerals show a distinct dominance of Nb over Ta; Ta/(Nb+Ta) ratios of 0.08–0.37, and negligible Ti content suggesting a low microlite and betafite components (Table 4, Fig. 6a). A large compositional variability exists for the actinides: 0.5–39.5 wt.% UO_2 and 0.5–16.3 wt.% ThO_2, however, the U,Th-richest compositions deviate significantly from the ideal pyrochlore stoichiometry. The pyrochlore grains display variable REE, Pb, and W contents; ≤9.3 wt.% REE_2O_3, ≤12.6 wt.% PbO, and ≤4.6 wt.% WO_3. A notoriously elevated concentration of SiO_2 (≤11.9 wt.%, exceptionally 17.2 wt.%) that correlates negatively with Σ(Nb, Ta) (Fig. 7), and low analytical totals indicate a strong hydration (Table 4).

Pyrochlore compositions usually show a constantly dominant *A*-cation vacancy (0.59–1.64 pfu), prevailing over U, Th, Fe^{2+}, REE, Ca and other cations in the *A* site (Fig. 6b). Fluorine content maximizes to 3.2 wt.% (0.47 apfu F). Therefore, according to the approved CNMNC–IMA nomenclature (Atencio et al. 2010), the pyrochlore supergroup minerals can

be classified as zero-valence-dominant pyrochlore, rarely unspecified uranium-dominant member of the pyrochlore group (designed as "uranpyrochlore").

Discussion

The Markersbach granite pluton forms the northeasternmost part of the Erzgebirge–Vogtland "batholith", one of the best-known metallogenetic provinces within the European Variscides, along with Cornwall (UK), the Massif Central (France), and the Iberian Massif (Portugal/Spain). Greisen-type, stockwork, skarn and vein-hosted mineralizations in the eastern area encompass (a) the world-class Cínovec (Zinnwald) Li–Sn–W deposit (Czech Republic/Germany) and spatially and genetically related satellite Li–(Sn–W) systems developed in granite cupolas, e.g., Krupka (Breiter & Frýda 1995; Breiter et al. 2017; Hreus et al. 2021; Krejčí Kotlanová et al. 2024), (b) Sn–Li–(W–Cu) prospects in Sadisdorf, Falkenhain, Sachsenhöhe, Hegelshöhe, and Altenberg prospect (Leopardi et al. 2024a, b; Burisch et al. 2025). Two geochemically contrasted late-Variscan granites occur in this metallogenic province: (i) strongly peraluminous S-type (ca. 325–315 Ma), showing a trend toward an increase in P, F, Rb, Li, U, Sn, W, Nb, and Ta combined with a decrease in HFSE and HREE, and (ii) slightly peraluminous A-type (ca. 325–295 Ma), very low in phosphorus, showing a trend toward an increase in F, Li, Rb, Be, Sn, W, Nb and Ta, associated with comparably larger contents of Zr, Th, Sc, As, Y and HREE (Förster et al. 1999; Hofmann et al. 2009; Breiter 2012). The Markersbach granite corresponds to aluminous, low-phosphorous granitic systems rich in REE, Y, Zr, and Hf. In addition to Li-micas and other accessory minerals (in particular zircon–thorite–coffinite–xenotime solid solutions, REE–Ca–Th fluorocarbonates and fluorides), the main minerals carrying rare metals in the Markersbach granite are Nb–Ta–W–Sn–Ti–Fe oxides (cassiterite, rutile, columbite and pyrochlore supergroup minerals). Besides from high-phosphorous, strongly peraluminous rare metal S-type granites, this oxide-mineral assemblage is also typical for low-phosphorous, HFSE-enriched, slightly peraluminous A-type granites (e.g., Belkasmi et al. 2000; Breiter et al. 2007; Breiter 2012; Zhao et al. 2021). In the Erzgebirge, this resembles the Markersbach intrusion and other shallowly emplaced granite occurrences in the eastern Erzgebirge (e.g., Johan & Johan 1994; Breiter et al. 2017; Hreus et al. 2021). Although the Markersbach granite rare-metal mineralization shares many similarities with other aluminous A-type granite systems of the Erzgebirge region, there are several specific differences in mineral chemistry and temporal evolution of Nb–Ta–W–Sn–Ti–Fe accessory minerals, which are discussed subsequently.

Table 3: Representative results of EPMA analyses and calculated mineral formulae of columbite-(Fe) (Clb). Note: n.a. – not analyzed; * = recalculated.

sample	1042	1096B	1096B		1042	1096B	1096B
mineral	Clb	Clb	Clb		Clb	Clb	Clb
WO_3 (wt.%)	6.22	2.49	2.32	W^{6+} (apfu)	0.093	0.037	0.034
Nb_2O_5	58.75	70.78	70.85	Nb^{5+}	1.536	1.816	1.825
Ta_2O_5	8.96	1.50	1.56	Ta^{5+}	0.141	0.023	0.024
SiO_2	-	0.01	0.00	Si^{4+}	0.000	0.000	0.000
TiO_2	5.01	2.17	2.10	Ti^{4+}	0.218	0.093	0.090
ZrO_2	0.23	0.10	0.14	Zr^{4+}	0.006	0.003	0.004
HfO_2	n.a.	0.03	0.00	Hf^{4+}	–	0.000	0.000
SnO_2	0.79	0.06	0.06	Sn^{4+}	0.018	0.001	0.001
ThO_2	n.a.	0.03	0.02	$\sum M1$	2.012	1.973	1.978
UO_2	0.07	0.00	0.00	Th^{4+}	–	0.000	0.000
Sc_2O_3	1.69	0.44	0.44	U^{4+}	0.001	0.000	0.000
Y_2O_3	0.09	0.07	0.00	Sc^{3+}	0.085	0.022	0.022
La_2O_3	n.a.	0.00	0.00	Y^{3+}	0.003	0.002	0.000
Ce_2O_3	n.a.	0.05	0.00	La^{3+}	–	0.000	0.000
Pr_2O_3	n.a.	0.20	0.15	Ce^{3+}	–	0.001	0.000
Nd_2O_3	n.a.	0.02	0.00	Pr^{3+}	–	0.004	0.003
Sm_2O_3	n.a.	0.07	0.01	Nd^{3+}	–	0.000	0.000
Eu_2O_3	n.a.	0.69	0.66	Sm^{3+}	–	0.001	0.000
Gd_2O_3	n.a.	0.11	0.13	Eu^{3+}	–	0.013	0.013
Tb_2O_3	n.a.	0.07	0.15	Gd^{3+}	–	0.002	0.003
Dy_2O_3	n.a.	0.11	0.06	Tb^{3+}	–	0.001	0.003
Ho_2O_3	n.a.	0.00	0.00	Dy^{3+}	–	0.002	0.001
Er_2O_3	n.a.	0.34	0.34	Ho^{3+}	–	0.000	0.000
Tm_2O_3	n.a.	0.07	0.12	Er^{3+}	–	0.006	0.006
Yb_2O_3	n.a.	0.16	0.20	Tm^{3+}	–	0.001	0.002
Lu_2O_3	n.a.	0.08	0.24	Yb^{3+}	–	0.003	0.003
Sb_2O_3	n.a.	0.01	0.00	Lu^{3+}	–	0.001	0.004
Fe_2O_3*	1.04	3.77	3.05	Sb^{3+}	–	0.000	0.000
FeO*	15.81	14.40	14.92	Fe^{3+}*	0.045	0.159	0.129
MnO	2.04	3.30	3.14	Fe^{2+}*	0.761	0.674	0.703
CaO	0.01	0.02	0.00	Mn^{2+}	0.100	0.159	0.152
ZnO	0.00	n.a.	n.a.	Ca^{2+}	0.001	0.001	0.000
MgO	0.00	0.02	0.01	Zn^{2+}	0.000	–	0.000
PbO	n.a.	0.00	0.00	Mg^{2+}	0.000	0.002	0.001
F	n.a.	0.10	0.12	Pb^{2+}	–	0.000	0.000
O=F	–	−0.02	−0.03	$\sum M2$	0.996	1.056	1.045
Total	100.70	101.24	100.76	Total	3.008	3.029	3.024
				Mn/(Mn+Fe)	0.196	0.160	0.154
				Ta/(Nb+Ta)	0.081	0.013	0.013

Crystal chemistry and accommodation of Nb, Ta, W, Sn and Si

The most characteristic feature of columbite supergroup minerals in the Markersbach granite as well as other Erzgebirge granites is the significant accommodation of W. A W-rich species analogous in composition to nioboixiolite series from the nearby Cínovec (Zinnwald) Sn–W–Li deposit, Czech Republic, was named W-rich columbite by Johan & Johan (1994) resp. W-rich ixiolite by Breiter et al. 2017 and a mineral phase with strong W-enrichment was identified as qitianlingite by Breiter et al. (2017) and Hreus et al. (2021). The Figure 5

Table 4: Representative results of EPMA analyses and calculated mineral formulae of pyrochlore (Pcl). The analyses of U–Nb–Ta phase and Nb-rich ferric oxide (Feox) are given at wt.% of oxides only. Note: n.a. – not analyzed.

sample	1047B	1047	1047	1047	1047	1047	1096	1096	1096		1047B	1047	1047	1047
spot in Fig. 2							5	6	7					
mineral	Pcl	Pcl	Pcl	Pcl	U–Nb–Ta	U–Nb–Ta	Feox	Feox	Feox		Pcl	Pcl	Pcl	Pcl
WO_3 (wt.%)	2.78	1.99	1.83	2.16	2.79	2.56	4.49	3.60	3.67	W^{6+} (apfu)	0.051	0.041	0.032	0.047
P_2O_5	0.00	3.57	n.a.	n.a.	2.30	1.71	n.a.	n.a.	n.a.	P^{5+}	0.000	0.240	–	–
Nb_2O_5	36.64	22.58	29.82	23.77	16.62	17.80	13.68	13.28	12.51	Nb^{5+}	1.174	0.812	0.920	0.901
Ta_2O_5	3.98	2.70	9.79	11.24	2.04	1.63	6.90	5.80	5.38	Ta^{5+}	0.077	0.058	0.182	0.256
Sb_2O_5	0.00	0.21	n.a.	n.a.	0.72	0.87	n.a.	n.a.	n.a.	Sb^{5+}	0.000	0.006	–	–
SiO_2	4.88	10.06	5.89	4.33	1.28	1.19	2.80	2.84	2.47	Si^{4+}	0.346	0.800	0.402	0.363
TiO_2	0.48	0.17	0.24	0.34	0.38	0.40	0.74	0.65	0.67	Ti^{4+}	0.026	0.010	0.012	0.021
ZrO_2	1.97	0.83	0.56	0.32	0.24	0.24	0.53	0.59	0.58	Zr^{4+}	0.068	0.032	0.019	0.013
HfO_2	0.14	0.00	0.17	0.15	0.00	0.00	n.a.	n.a.	n.a.	Hf^{4+}	0.003	0.000	0.003	0.004
SnO_2	0.11	0.03	0.20	0.17	0.00	0.00	2.08	1.93	1.68	Al^{3+}	0.252	0.000	0.423	0.006
ThO_2	11.37	2.53	2.16	0.94	2.06	1.27	n.a.	n.a.	n.a.	Sn^{4+}	0.003	0.001	0.005	0.389
UO_2	11.10	25.82	17.24	30.56	39.54	44.66	0.11	0.11	0.21	$\sum B$	2.000	2.000	2.000	2.000
Al_2O_3	3.02	0.00	5.26	3.93	n.a.	n.a.	1.36	1.49	1.74	U^{4+}	0.180	0.457	0.262	0.570
Sc_2O_3	0.04	0.08	0.09	0.06	0.05	0.02	0.37	0.31	0.32	Th^{4+}	0.179	0.046	0.034	0.018
Y_2O_3	1.23	1.20	0.46	0.33	1.20	2.10	0.30	0.42	0.70	Sc^{3+}	0.003	0.005	0.006	0.005
La_2O_3	0.15	n.a.	0.17	0.14	n.a.	n.a.	n.a.	n.a.	n.a.	Y^{3+}	0.046	0.051	0.017	0.015
Ce_2O_3	2.80	1.36	1.05	0.88	3.55	2.11	n.a.	n.a.	n.a.	$\sum Ln^{3+}$	0.194	0.040	0.087	0.096
Pr_2O_3	0.29	n.a.	0.28	0.25	n.a.	n.a.	n.a.	n.a.	n.a.	Fe^{2+}	0.200	0.181	0.128	0.146
Nd_2O_3	0.40	n.a.	0.36	0.21	n.a.	n.a.	n.a.	n.a.	n.a.	Mn^{2+}	0.021	0.043	0.027	0.016
Sm_2O_3	0.22	n.a.	0.13	0.07	n.a.	n.a.	n.a.	n.a.	n.a.	Ca^{2+}	0.044	0.062	–	–
Eu_2O_3	0.16	n.a.	0.24	0.31	n.a.	n.a.	n.a.	n.a.	n.a.	Zn^{2+}	0.000	0.000	–	–
Gd_2O_3	0.38	n.a.	0.31	0.30	n.a.	n.a.	n.a.	n.a.	n.a.	Mg^{2+}	0.003	0.005	0.075	0.093
Tb_2O_3	0.17	n.a.	0.04	0.10	n.a.	n.a.	n.a.	n.a.	n.a.	Pb^{2+}	0.000	0.045	0.147	0.134
Dy_2O_3	1.17	n.a.	0.12	0.08	n.a.	n.a.	n.a.	n.a.	n.a.	Na^{+}	0.000	0.000	0.009	0.015
Ho_2O_3	0.22	n.a.	0.02	0.01	n.a.	n.a.	n.a.	n.a.	n.a.	$\sum A$	0.875	0.934	0.794	1.111
Er_2O_3	1.01	n.a.	0.37	0.30	n.a.	n.a.	n.a.	n.a.	n.a.	$^{A}\square$	1.125	1.066	1.206	0.889
Tm_2O_3	0.16	n.a.	0.27	0.30	n.a.	n.a.	n.a.	n.a.	n.a.	O	6.000	6.000	6.000	6.000
Yb_2O_3	0.73	n.a.	0.34	0.20	n.a.	n.a.	n.a.	n.a.	n.a.	^{X}OH	0.000	0.000	0.000	0.000
Lu_2O_3	0.24	n.a.	0.00	0.24	n.a.	n.a.	n.a.	n.a.	n.a.	$\sum X$	6.000	6.000	6.000	6.000
Fe_2O_3	–	–	–	–	–	–	57.08	58.31	58.46	K^{+}	0.000	0.000	0.004	0.007
FeO	3.75	3.02	2.49	2.32	1.89	1.59	–	–	–	F	0.081	0.133	0.072	0.189
MnO	0.35	0.63	0.46	0.23	0.15	0.19	0.54	0.46	0.47	Cl	–	–	0.007	0.004
CaO	0.69	0.86	n.a.	n.a.	1.30	1.11	0.10	0.11	0.12	^{Y}OH	0.000	0.000	0.000	0.000
ZnO	0.00	0.00	n.a.	n.a.	0.00	0.00	0.04	0.03	0.03	^{Y}O	0.000	0.106	0.000	0.166
MgO	0.02	0.03	0.57	0.58	0.03	0.03	0.02	0.00	0.00	$^{Y}\square$	0.919	0.761	0.916	0.635
PbO	0.00	2.72	10.41	7.69	0.21	0.29	n.a.	n.a.	n.a.	$\sum Y$	1.000	1.000	1.000	1.000
Na_2O	0.00	0.00	0.05	0.07	n.a.	n.a.	n.a.	n.a.	n.a.	Nb+Ta	1.251	0.870	1.102	1.158
F	0.43	0.64	0.40	0.86	0.96	0.97	n.a.	n.a.	n.a.	U+Th	0.359	0.503	0.295	0.588
Cl	n.a.	n.a.	0.06	0.03	n.a.	n.a.	n.a.	n.a.	n.a.					
O=F	−0.18	−0.26	−0.17	−0.36	−0.40	−0.40	–	–	–					
O=Cl	–	–	−0.03	−0.01	–	–	–	–	–					
Total	90.90	80.75	91.67	93.08	76.88	80.32	91.12	89.94	89.01					

demonstrates the systematic and gradual enrichment of W from columbite-(Fe) via nioboixiolite I, qitianlingite to nioboixiolite II ("wolframoixiolite"). The significant W contribution facilitated the substitution of Fe^{3+} in the *M*2 site in columbite group minerals according to the substitution reaction $2W^{6+}+Fe^{3+}=3(Nb, Ta)^{5+}$, implying a possible redox-controlled evolution during consecutive mineral crystallization. The increased content of M^{4+} (Sn^{4+}, Ti^{4+} and Zr^{4+}) in columbite-(Fe) and nioboixiolite series indicates the additional occurrence of the substitution mechanism $W^{6+}+M^{4+}=2(Nb, Ta)^{5+}$ (cf. Johan & Johan 1994). The presence of this substitution is also supported by the similarity of ionic radii of the involved elements in octahedral six-fold coordination (Nb^{5+} and Ta^{5+}=0.64, Sn^{4+}=0.69, W=0.60 Å; Shannon 1976). Although the melt was tungsten-rich, W got almost entirely substituted into the columbite supergroup minerals during the magmatic stage. There is no indication of the occurrence of either magmatic or hydrothermal wolframite in the Markersbach granite. However, the widespread presence of nioboixiolite II ("wolframoixiolite") arises the question whether "wolframoixiolite" is really a homogenous, single mineral or rather a (nano)mixture of ferberite (wolframite) with columbite (Borneman-Starynkevitch et al. 1974; Chukanov et al. 2023). The limited miscibility and discontinuous trend between nioboixiolite

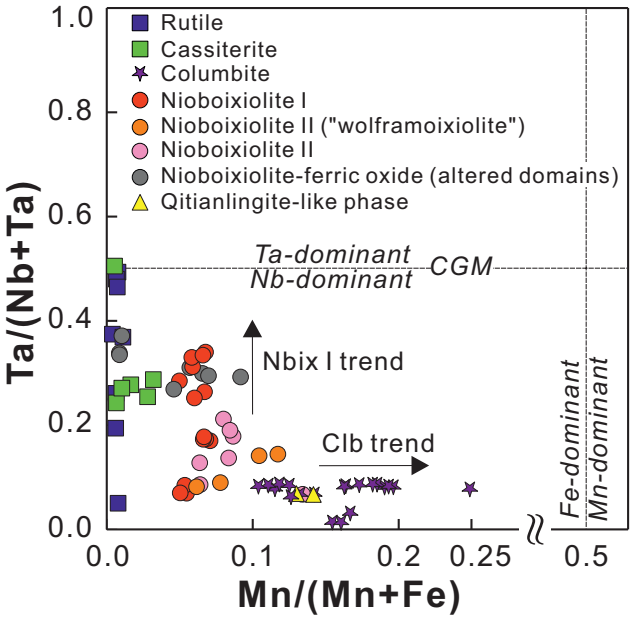

Fig. 3. Comparison of the atomic Mn/(Mn+Fe) and Ta/(Nb+Ta) values in the Nb–Ta–W–Sn–Ti–Fe mineral assemblage in the Markersbach granite. Grey circles are plotted as at. wt.%.

series and wolframite end-members are in line with what have been observed in the adjacent Cínovec granite, but differ from the observations in the strongly fractionated, P-rich Podlesí granite stock. In the latter, dominantly magmatic origin without pervasive hydrothermal reequilibration is considered (cf. Breiter et al. 2007, 2017), while crystallization of nioboixiolite II during the F-rich fluid-driven regime is expected in the Markersbach granite.

Conversely, the incorporation of Nb and Ta in rutile and cassiterite is generally interpreted as being due to the existence of a solid solution between TiO_2 (SnO_2) and columbite supergroup minerals $(Fe,Mn)(Nb,Ta)_2O_6$ (Clark & Fejer 1978; Černý & Ercit 1985; Möller et al. 1988). Hence, the presence of the $(Fe,Mn)^{2+}(Nb,Ta)_2(Ti,Sn)_{-3}$ and $Fe^{3+}(Nb,Ta)(Ti,Sn)_{-2}$ substitution vectors (Fig. 4b), leading to columbite-(Fe) and nioboixiolite-(Fe^{3+})/rossovskyite end-members, respectively, and their Ti–Sn-dominant counterparts are inferred (cf. Johan & Johan 1994; Černý et al. 1998, 1999; Chukanov et al. 2023, in press) (Fig. 5).

The accommodation and nature of Si in the pyrochlore supergroup minerals is still an unresolved problem. Pyrochlore-supergroup minerals that exhibit high Si content are reported from various evolved granite to pegmatite and carbonatite rocks (e.g., Uher et al. 1998; Chakmouradian & Mitchell 2002; Bindi et al. 2006; Atencio et al. 2010; Viladkar & Sorokhtina 2021; Breiter et al. 2024), and these are frequently observed also in the Erzgebirge granites, particularly in the Cínovec (Zinnwald) granite cupola (Johan & Johan 1994; Rub et al. 1998; Breiter et al. 2017). Despite the absence of tetrahedral sites suitable for Si accommodation in the pyrochlore structure, some of the Si could be incorporated as Si^{4+} cation in the octahedral 6-coordinated *B* site, correlating negatively with Nb, Ta, W, Ti, Sn, and Zr (Subramanian et al. 1983; Johan & Johan 1994; Bonazzi et al. 2006; Atencio 2022). According to TEM-EDX research and crystal chemistry of pyrochlore from nepheline syenite of the Mariupol Massif, SE Ukraine, no more than 50 % of the Si measured by EPMA occupies the octahedral sites; a larger fraction (50–70 %) is located in radiation-damaged (metamict) domains or chemically altered portions (Atencio et al. 2010; Dumanska-Słowik et al. 2014). However, the absence of Si in the 6-coordinated *B* site is indicated by the lack of any $^{[6]}Si^{4+}$ signal in the MAS-NMR spectrum and, conversely, an amorphous species with tetrahedrally coordinated Si was identified (Dumanska-Słowik et al. 2014). The latter, however, does not fully correspond to our findings in the Markersbach granite, because the relatively chemically heterogeneous zero-valence-dominant pyrochlore minerals with varying (Nb+Ta) composition (Table 4; Figs. 5 and 6a) also reveal a highly variable Si content and a clearly negative

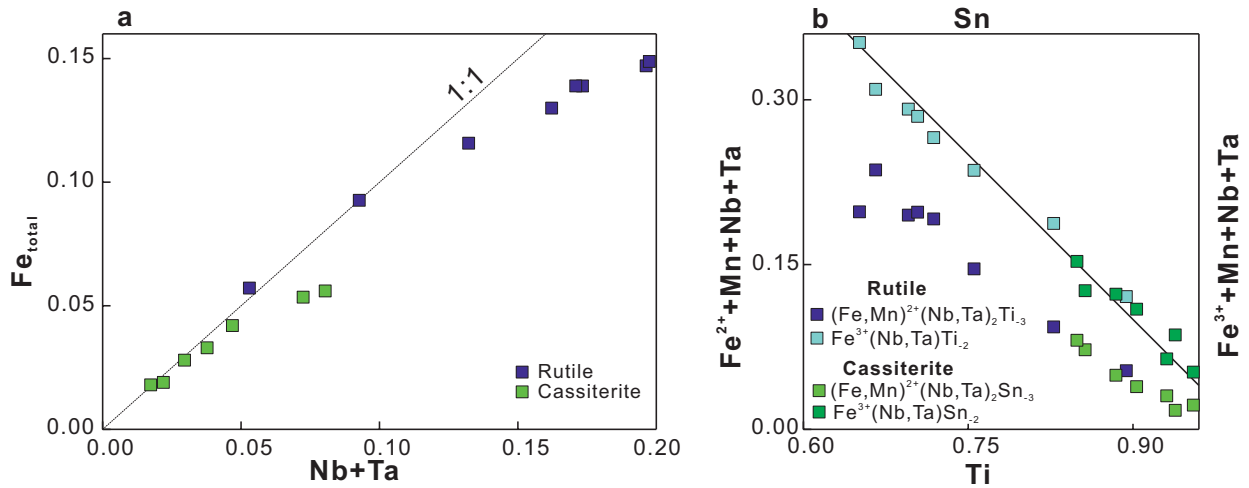

Fig. 4. Substitution diagrams (atomic proportions) of rutile and cassiterite from the Markersbach granite: **a** — (Nb+Ta) vs. total Fe; **b** — Ti vs. (Fe^{2+}+Mn+Nb+Ta) (in rutile) and Sn vs. (Fe^{3+}+Mn+Nb+Ta) (in cassiterite).

correlation between Nb+Ta and Si (Fig. 7). This circumstance most likely suggests the substantial presence of structurally accommodated Si on *B* site in the pyrochlore supergroup minerals discussed here (cf. Chakmouradian & Mitchell 2002; Breiter et al. 2024). Here, however, the presence of submicroscopic inclusions of any SiO_2 phase cannot be ruled out, especially in domains with ~17 wt.% SiO_2. On the contrary, uranium-dominant pyrochlore-like phase (U–Nb–Ta phase) from Markersbach have an obvious deviation from the ideal pyrochlore stoichiometry, suggesting its metamict state and non-structurally controlled accommodation of Si. Moreover, the U–Nb–Ta phase most probably represents the mixture of hydrated and amorphous (metamict) U,Th oxides and pyrochlore domains. The calculation of the pyrochlore empirical formula indicates the defect nature of the zero-valence-dominant pyrochlores. The fact that the *Y* site, occupied by F, Cl, OH, O, and K, remains almost vacant is corroborated by the low F content, although crystallized in a fluorine-rich environment (2100–8300 ppm F in the Markersbach granite, see section Geological and geochemical background) (cf. Johan & Johan 1994).

Magmatic versus hydrothermal origin

Valuable indicators of the fractionation of rare metal granitic magmas and associated pegmatitic melts include the Ta/(Nb+Ta) and Mn/(Fe+Mn) molar ratios in columbite supergroup minerals, usually evolving from Nb–Fe-dominant to Ta–Mn-rich (dominant) endmembers with progressing melt differentiation (e.g., Černý et al. 1985, 1986). These ratios are controlled by several factors, including the aluminium saturation index (ASI), overall composition of the parental melt, temperature, and different solubilities of $FeNb_2O_6$ and $MnTa_2O_6$ in the melt (e.g., Linnen & Keppler 1997; Fiege et al. 2011). The rim zones of columbite from evolved granites are usually characterized by Ta-enrichment and are associated with Li-micas, thus suggesting precipitation from Li–F-rich melt and coexisting fluids. However, some exceptions, or a more complex chemical evolution occur, which reflects combined effects of melt and fluid phase composition (e.g., Johan & Johan 1994; Belkasmi et al. 2000; Novák et al. 2003;

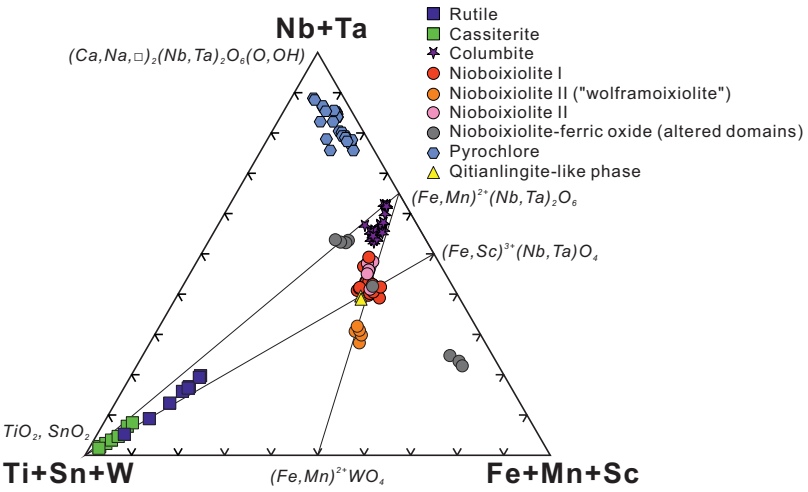

Fig. 5. Ternary (Nb+Ta) vs. (Ti+Sn+W) vs. (Fe+Mn+Sc) diagram (atomic proportions) showing the miscibility of columbite and pyrochlore supergroup solid solutions indicated by straight lines. Grey circles are plotted as at. wt. %.

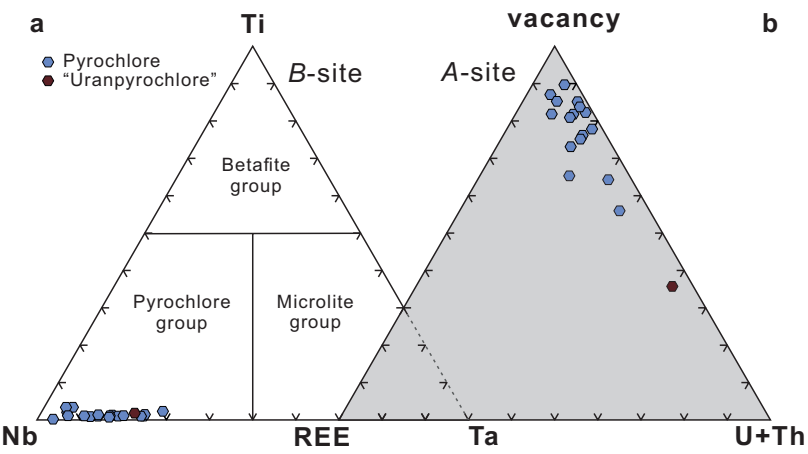

Fig. 6. Ternary diagrams illustrating the sites occupancy in the pyrochlore supergroup minerals from the Markersbach granite. **a** — *B* site: Nb–Ta–Ti distribution; **b** — *A* site: REE–U+Th-vacancy distribution.

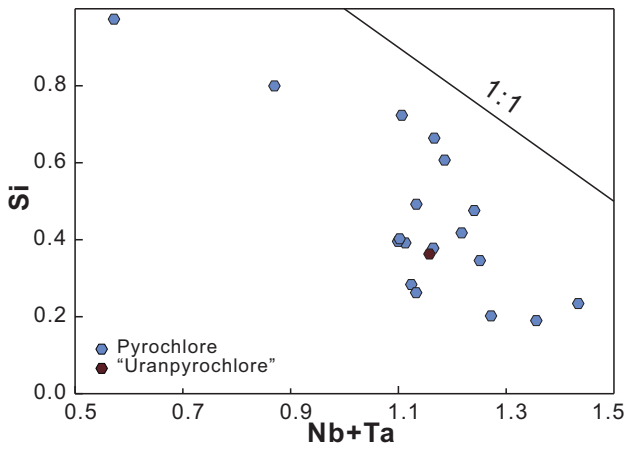

Fig. 7. Substitution Si vs. (Nb+Ta) diagram (atomic proportions) of pyrochlore supergroup minerals from the Markersbach granite.

Van Lichtervelde et al. 2006; Chudík et al. 2011; Wise et al. 2012; Neiva et al. 2015; Chládek et al. 2020). Columbite-(Fe) from the Markersbach granite shows limited, but recognizable Mn/(Fe+Mn) variations and a nearly constant Ta/(Nb+Ta) ratio, while nioboixiolite I displays a different evolutional trend, with negligible Mn/(Fe+Mn) and wide Ta/(Nb+Ta) variations (Fig. 3). A similar compositional trend for columbites was observed in the nearby Cínovec (Zinnwald) aluminous A-type granite (Rub et al. 1998; Breiter et al. 2017). Other occurrences of columbite group minerals sharing this trend include Sn–W-bearing rare metal granites, e.g., in the Eastern Desert, Arabian–Nubian Shield, Egypt (Abdalla et al. 1998), Gemeric specialized S-type granites, Slovakia (Uher et al. 2001), as well as in NYF pegmatites of the Grenville Province (Ercit 1994) or LCT pegmatites from Mount Begbie, British Columbia, Canada (Dixon et al. 2014). Most rare-element granite pegmatites show trends characterized by strongly increasing Ta/(Nb+Ta) ratios from columbite to tantalite (e.g., Černý et al. 1986; Lahti 1987; Wise et al. 2012). The different Mn/(Fe+Mn) and Ta/(Nb+Ta) evolution in nioboixiolite compared to columbite-(Fe) from the Markersbach granite reveals a possible reverse trend in nioboixiolite, distinguished by an increased Nb content in grain rims and, thus, a reverse zonation in terms of Ta/(Nb+Ta) and Mn/(Fe+Mn) (Figs. 2b, 3). This suggests a change of the conditions in the magma and probably marks the point from purely magmatic conditions during nioboixiolite crystallization towards the post-magmatic stage, i.e., from primarily melt-dominated to a more fluid-driven regime (cf. Michaud & Pichavant 2020), but still under flux-rich late magmatic conditions. Conversely, the trend of Mn/(Fe+Mn) in the columbite-(Fe) reflects mainly the post-magmatic evolution, which results from in-situ metasomatic replacement processes related to fluids and limited Nb/Ta fluctuation.

An interesting Fe–Mn correlation is observed between the evolution of columbite supergroup minerals and the associated micas. The Fe-dominant signature can be readily explained in terms of the Fe and Mn budget in Li–Fe micas and whole rock (cf. Breiter et al. 2019). The Li-rich annite to siderophyllite (zinnwaldite) is the major host of Fe and Mn, since garnet, tourmaline and/or fluorapatite, minerals important in triggering the Mn/Fe fractionation, do not occur in the Markersbach granite. The values of Mn/(Fe+Mn)=0.02–0.03 in Li-rich micas are similar to those recorded in the whole rock (≤0.04), implying that the crystallization of accessory minerals did not significantly modify this value. The Mn/Fe ratio of the melt was stabilized during the crystallization of the Fe–Li micas. Columbite supergroup minerals incorporated both Fe and Mn in proportions nearly identical to those of the melt (cf. Breiter et al. 2017). On the other hand, columbite supergroup minerals exert a major control on the Nb/Ta fractionation in the melt, while the share of trioctahedral mica in the bulk-rock budget of Nb, Ta decreases from 40–70 % in biotite granite to ≤5 wt. % in greisen (Breiter et al. 2019). The relatively higher solubility of Ta in a Li–F-rich environment (Linnen 1998) caused a systematic core-to-rim Ta enrichment during the transition from magmatic to hydrothermal conditions (Rub et al. 1998; Xie et al. 2016). Among all Nb–Ta–W–Sn–Ti–Fe accessory minerals studied herein, the highest Ta/(Nb+Ta) values were observed in cassiterite (≤0.51) and rutile (≤0.49) (Fig. 3), while columbite supergroup minerals show a rather smaller degree of Nb/Ta fractionation.

As revealed from mineral chemistry, the formation of Nb–Ta–W–Sn–Ti–Fe oxides within the Markersbach granite took place during different growth stages, supporting their magmatic-hydrothermal origin. A high degree of fractional crystallization of the Markersbach granite magma and/or the low degree anatectic melting of an already enriched protolith are likely the main factors facilitating the already magmatic enrichment of rare metals. This allowed the saturation of columbite supergroup minerals instead of the crystallization of Ti oxides and silicates (ilmenite, rutile, and titanite) which constitute the major hosts of rare metals in less evolved granites. This initial enrichment of rare metals and the higher fractionation degree is supported by low whole rock Zr/Hf value (≤16.6) and moderately lower Nb/Ta ratio (3.8–8.6). Anyway, the composition of the Markersbach granites and compositional-textural evolution of Nb–Ta–W–Sn–Ti–Fe minerals cannot be explained in terms of simple crystal fractionation but involves significant element remobilization and intra-granitic redistribution during fluid–rock interaction (cf. Förster 2001; Štemprok et al. 2003). A whole-rock Nb/Ta ratio of ≥5 combined with Zr/Hf ratio of ≥26 is defined as an ideal boundary value of barren granites whose composition is derived from magmatic fractionation only, while rocks with Nb/Ta<5, Zr/Hf<~25 and K/Rb ratio of <150 have additionally been influenced by magmatic–post-magmatic fluids and represent granites that are spatially related to Sn–W(–U) or rare-metal mineralization (Ballouard et al. 2016). However, Markersbach granite with Nb/Ta>5, Zr/Hf<18 and K/Rb≤100 fall out of the classification, possibly indicating a loss of the signature of metallic enrichment through significant magmatic fractionation postdated by subsolidus hydrothermal alteration associated with a relatively limited rare metal remobilization. Consequently, even if the degree of magmatic fractionation was reasonably high in the Markersbach granite, the individual Nb/Ta fractionation was lower and absolute abundances of rare metals were lower relative to F-rich true and fertile rare metal granites. This limited rare metal fractionation during magmatic–hydrothermal processes is corroborated by the absence of Ta-dominant columbite supergroup minerals and lower absolute abundances of Sn (≤30 ppm), Cs (≤35 ppm) and W (≤15 ppm), geochemical markers distinguishing fertile rare metal granites having an economically relevant metallogenetic potential (cf. Ballouard et al. 2016). The explanation could be the unambiguous low content of Li in Markersbach granite, only rarely exceeding 400 ppm, which suppressed Nb/Ta fractionation (cf. Breiter et al. 2007).

In summary, considering the textural observations and variations in Ta/(Nb+Ta) and Mn/(Fe+Mn) values in the Nb–Ta minerals, the oscillatory zoned nioboixiolite I and small disseminated, compositionally homogenous, columbite-

(Fe) most probably crystallized from the late granitic melt as a result of variable growth rates, fluctuating equilibrium or rather disequilibrium fractional crystallization, localized saturation, and Nb/Ta fluctuation (Lahti 1987; Johan & Johan 1994; Van Lichtervelde et al. 2018). The reverse Ta/(Nb+Ta) trend observed in the Nb-rich outer zones of nioboixiolite I indicates a complex fluid–melt interactions (Černý et al. 1986; London 2008). The W-rich patchy marginal domains of nioboixiolite II ("wolframoixiolite"), the Nb–Ta rich porous cassiterite and rutile are probably of late-magmatic to early post-magmatic origin within a F-rich environment. It is not yet clear, when exactly the patchy zoning in originally magmatic columbite-(Fe) developed, what elements were enriched in the alteration fluid, and what was the intensity of elemental leaching from the columbite-(Fe). However, a marginal, W-rich qitianlingite-like phase appears as late-stage mineral partly replacing columbite-(Fe) and evolutionary correlates to nioboixiolite II ("wolframoixiolite"). Such patchy zoned columbite cores reflecting strong, irregular variations in W content, were also reported from the south-westerly Cínovec/Zinnwald granite cupola (Johan & Johan 1994; Breiter et al. 2017). Finally, lower temperature fluids induced the partial dissolution of primary ore minerals combined with a minor remobilization of rare metals, giving rise to pyrochlore supergroup minerals and Nb(Ta)-enriched ferric oxide (goethite?). This ferric oxide represents the latest formed rare-metal bearing phase and a unique secondary host of the geochemically relatively low mobile Nb. This suggests that Nb mobility may be more complex than previously thought, and its use as a truly invariant element may be limited. It also indicates the possible capacity of F-rich fluids effectively mobilize and transport Nb and Ta (e.g., Akinfiev et al. 2020).

Acknowledgements: This publication is sincerely dedicated to our colleague and friend, Igor Broska, who constantly inspires, supports, and helps us to make our research and life even better. We are grateful for the opportunity to contribute to the special issue "Accessory minerals: tracers of petrogenesis" dedicated to his scientific contributions. This work was supported by the Slovak Research and Development Agency under the contract APVV-22-0092. We are grateful to Tomáš Mikuš, Sergii Kurylo, Matej Rybárik and Patrik Konečný for their assistance during the analytical works. We thank Karel Breiter, Adam Pieczka, Sebastián Hreus and Štepán Chládek (reviewers) and Milan Kohút (Associate Editor) for their constructive suggestions.

References

Abdalla H.M., Helba H.A. & Mohamed F.H. 1998: Chemistry of columbite-tantalite minerals in rare metal granitoids, Eastern Desert, Egypt. *Mineralogical Magazine* 62, 821–836. https://doi.org/10.1180/002646198548197

Akinfiev N.N., Korzhinskaya V.S., Kotova N.P., Redkin A.F. & Zotov A.V. 2020: Niobium and tantalum in hydrothermal fluids: Thermodynamic description of hydroxide and hydroxofluoride complexes. *Geochimica et Cosmochimica Acta* 280, 102–115. https://doi.org/10.1016/j.gca.2020.04.009

Åmli R. & Griffin W.L. 1975: Microprobe analysis of REE minerals using empirical correction factors. *American Mineralogist*, 60, 599–606.

Atencio D. 2022: Crystal chemistry and phase transitions in pyrochlore and related structures. In: Chowdhury A. (Ed.): Pyrochlore Ceramics: Properties, Processing, and Applications. *Elsevier Series on Advanced Ceramic Materials.* Amsterdam, 3–24. https://doi.org/10.1016/B978-0-323-90483-4.00001-5

Atencio D., Andrade M.B., Christy A.G., Gieré R. & Kartashov P.M. 2010: The pyrochlore supergroup of minerals: nomenclature. *Canadian Mineralogist* 48, 673–698. https://doi.org/10.3749/canmin.48.3.673

Ballouard C., Poujol M., Boulvais P., Branquet Y., Tartese R. & Vigneresse J.-L. 2016: Nb–Ta fractionation in peraluminous granites: a marker of the magmatic–hydrothermal transition. *Geology* 44, 231–234. https://doi.org/10.1130/G37475.1

Belkasmi M., Cuney M., Pollard P.J. & Bastoul A. 2000: Chemistry of the Ta–Nb–Sn–W oxide minerals from the Yichun rare metal granite (SE China): genetic implications and comparison with Moroccan and French Hercynian examples. *Mineralogical Magazine* 64, 507–523. https://doi.org/10.1180/002646100549391

Bindi L., Zoppi M. & Bonazzi P. 2006: Plumbomicrolite from the Ploskaya Mountain, Keivy massif, Kola peninsula, Russia: Composition and crystal structure. *Periodico di Mineralogia* 75, 51–58.

Bonazzi P., Bindi L., Zoppi M., Capitani G.C. & Olmi F. 2006: Single-crystal diffraction and transmission electron microscopy studies of silicified pyrochlore from Narssâtssuk, Julianehaab district, Greenland. *American Mineralogist* 91, 794–801. https://doi.org/10.2138/am.2006.1777

Borneman-Starynkevitch I.D., Rudnitskaya E.S., Loseva T.I. & Amelina V.S. 1974: Once again, wolframoixiolite. *Sbornik Nauchnykh Trudov Moskovskogo Otdeleniya Vsesoyuznogo Mineralogicheskogo Obshchestva* 1974, 25–28 (in Russian).

Bosi F., Hatert F., Pasero M. & Mills S. 2024: IMA Commission on New Minerals, Nomenclature and Classification (CNMNC) – Newsletter 82. *European Journal of Mineralogy* 36, 1005–1010. https://doi.org/10.5194/ejm-36-1005-2024

Breiter K. 2012: Nearly contemporaneous evolution of the A- and S-type fractionated granites in the Krušné hory/Erzgebirge Mts., Central Europe. *Lithos* 151, 105–121. https://doi.org/10.1016/j.lithos.2011.09.022

Breiter K. & Frýda J. 1995: The Krupka tin deposit. In: Breiter K. & Seltmann R. (Eds.): Excursion guide: mineralizations of the Krušné hory Mts. (Erzgebirge). *3rd SGA Meeting, Czech Geological Survey*, Prague, 103–112.

Breiter K., Förster H.J. & Seltmann R. 1999: Variscan silicic magmatism and related tin- tungsten mineralization in the Erzgebirge-Slavkovský les metallogenic province. *Mineralium Deposita* 34, 505–521. https://doi.org/10.1007/s001260050217

Breiter K., Škoda R. & Uher P. 2007: Nb–Ta–Ti–W–Sn-oxide minerals as indicators of a peraluminous P- and F-rich granitic system evolution: Podlesí, Czech Republic. *Mineralogy and Petrology* 91, 225–248. https://doi.org/10.1007/s00710-007-0197-1

Breiter K., Korbelová Z., Šešulka V. & Honig S. 2016: New rock and mineral data from the Li(Sn,W,Nb,Ta)-deposit Cínovec–jih. *Geoscience Research Reports* 49, 113–121.

Breiter K., Korbelová Z., Chládek Š., Uher P., Knesl I., Rambousek P., Honig S. & Šešulka V. 2017: Diversity of Ti–Sn–W–Nb–Ta

oxide minerals in the classic granite-related magmatic–hydrothermal Cínovec/Zinnwald Sn–W–Li deposit (Czech Republic). *European Journal of Mineralogy* 29, 727–738. https://doi.org/10.1127/ejm/2017/0029-2650

Breiter K., Hložková M., Korbelová Z. & Vašinová Galiová M. 2019: Diversity of lithium mica compositions in mineralized granite–greisen system: Cínovec Li–Sn–W deposit, Erzgebirge. *Ore Geology Reviews* 106, 12–27. https://doi.org/10.1016/j.oregeorev.2019.01.013

Breiter K., Costi H.T. & Korbelová Z. 2024: Pyrochlore-supergroup minerals and their relation to columbite-group minerals in peralkaline to subaluminous A-type rare-metal granites with special emphasis on the Madeira pluton, Amazonas, Brazil. *Minerals* 14, 1302.

Burisch M., Leopardi D., Guilcher M., Šešulka V., Dittrich T. & Lehmann B. 2025: Greisen-hosted lithium resources of the Erzgebirge/Krušné Hory province (Germany and Czech Republic). *Economic Geology* 120, 627–647. https://doi.org/10.5382/econgeo.5136

Černý P. & Ercit T.S. 1985: Some recent advances in the mineralogy and geochemistry of Nb and Ta in rare-element granitic pegmatites. *Bulletin de Minéralogie* 108, 499–532.

Černý P., Meintzer R.E.& Anderson A.J. 1985: Extreme fractionation in rare-element granitic pegmatites: selected examples of data and mechanisms. *Canadian Mineralogist* 23, 381–421.

Černý P., Goad B.E., Hawthorne F.C. & Chapman R. 1986: Fractionation trends of the Nb- and Ta-bearing oxide minerals in the Greer Lake pegmatitic granite and its pegmatite aureole, southeastern Manitoba. *American Mineralogist* 71, 501–517.

Černý P. & Ercit T.S., Wise M.A., Chapman R. & Buck H.M. 1998: Compositional, structural and phase relationships in titanian ixiolite and titanian columbite–tantalite. *Canadian Mineralogist* 36, 547–561.

Černý P. Chapman R., Simmons W.B. & Chackowsky L.E. 1999: Niobian rutile from the McGuire granitic pegmatite, Park County, Colorado: Solid solution, exsolution, and oxidation. *American Mineralogist* 84, 754–763. https://doi.org/10.2138/am-1999-5-607

Černý P., Blevin P.L., Cuney M. & London D. 2005: Granite-related ore deposits. *Economic Geology 100th Anniversary volume*, 337–370.

Chakmouradian A.R. & Mitchell R.H. 2002: New data on pyrochlore- and perovskite-group minerals from the Lovozero alkaline complex, Russia. *European Journal of Mineralogy* 14, 821–836.

Chappell B.W. 1999: Aluminium saturation in I- and S-type granites and the characterization of fractionated haplogranites. *Lithos* 46, 535–551. https://doi.org/10.1016/S0024- 4937(98)00086-3

Chládek Š., Uher P. & Novák M. 2020: Compositional and textural variations of columbite-group minerals from beryl–columbite pegmatites in the Maršíkov district, Bohemian Massif, Czech Republic: Magmatic versus hydrothermal evolution. *Canadian Mineralogist* 58, 767–783. https://doi.org/10.3749/canmin.1900093

Chudík P., Uher P., Gadas P., Škoda R. & Pršek J. 2011: Niobium–tantalum oxide minerals in the Jazuitské Lesy granitic pegmatite, Bratislava Massif, Slovakia: Ta to Nb and Fe to Mn evolutionary trends in a narrow Be,Cs-rich and Li,B-poor dike. *Mineralogy and Petrology* 102, 15–27. https://doi.org/10.1007/s00710-011-0163-9

Chukanov N.V., Pasero M., Aksenov S.M., Britvin S.N., Zubkova N.V., Yike L. & Witzke T. 2023: Columbite supergroup of minerals: nomenclature and classification. *Mineralogical Magazine* 87, 18–33. https://doi.org/10.1180/mgm.2022.105

Chukanov N.V., Zubkova N.V., Pekov I.V., Kasatkin A.V., Agakhanov A.A., Virus A.A., Vigasina M.F., Ternes B., Schüller W. & Britvin S., in press: Nioboixiolite-(Fe^{3+}), ($Nb_{0.5}Fe^{3+}_{0.5}$)O_2, a new ixiolite-group mineral from the Eifel paleovolcanic region, Germany. *Mineralogical Magazine.* https://doi.org/10.1180/mgm.2025.15

Clark A.M. & Fejer E.E. 1978: Tapiolite, its chemistry and cell dimensions. *Mineralogical Magazine* 42, 477–480. https://doi.org/10.1180/minmag.1978.042.324.09

Dixon A., Cempírek J. & Groat L.A. 2014: Mineralogy and geochemistry of pegmatites on Mount Begbie, British Columbia. *Canadian Mineralogist* 52, 129–164. https://doi.org/10.3749/canmin.52.2.129

Dumanska-Słowik M., Pieczka A., Tempesta G., Olejniczak Z. & Heflik W. 2014: "Silicified" pyrochlore from nepheline syenite (mariupolite) of the Mariupol Massif, SE Ukraine: A new insight into the role of silicon in the pyrochlore structure. *American Mineralogist* 99, 2008–2017. https://doi.org/10.2138/am-2014-4896

Ercit T.S. 1994: The geochemistry and crystal chemistry of columbite-group minerals from granitic pegmatites, southwestern Greenville Province, Canadian Shield. *Canadian Mineralogist* 32, 421–438.

Fiege A., Kirchner C., Holtz F., Linnen, R.L. & Dziony W. 2011: Influence of fluorine on the solubility of manganotantalite ($MnTa_2O_6$) and manganocolumbite ($MnNb_2O_6$) in granitic melts – An experimental study. *Lithos* 122, 165–174. https://doi.org/10.1016/j.lithos.2010.12.012

Förster H.J. 1998a: The chemical composition of REE–Y–Th–U-rich accessory minerals in peraluminous granites of the Erzgebirge–Fichtelgebirge region, Germany, Part I: The monazite-(Ce)-brabantite solid solution series. *American Mineralogist* 83, 259–272. https://doi.org/10.2138/am-1998-3-409

Förster H.J. 1998b: The chemical composition of REE–Y–Th–U-rich accessory minerals in peraluminous granites of the Erzgebirge–Fichtelgebirge region, Germany. Part II: Xenotime. *American Mineralogist* 83, 1302–1315. https://doi.org/10.2138/am-1998-11-1219

Förster H.J. 1999: The chemical composition of uraninite in Variscan granites of the Erzgebirge, Germany. *Mineralogical Magazine* 63, 239–252. https://doi.org/10.1180/002646199548466

Förster H.J. 2001: Synchysite-(Y)–synchysite-(Ce) solid solutions from Markersbach, Erzgebirge, Germany: REE and Th mobility during high-T alteration of highly fractionated aluminous A-type granites. *Mineralogy and Petrology* 72, 259–280. https://doi.org/10.1007/s007100170019

Förster H.J. 2006: Composition and origin of intermediate solid solutions in the system thorite–xenotime–zircon–coffinite. *Lithos* 88, 35–55. https://doi.org/10.1016/j.lithos.2005.08.003

Förster H.J., Tischendorf G., Trumbull R.B. & Gottesmann B. 1999: Late-collisional granite magmatism in the Variscan Erzgebirge, Germany. *Journal of Petrology* 40, 1613–1645. https://doi.org/10.1093/petroj/40.11.1613

Förster H.J., Ondrejka M. & Uher P. 2011: Mineralogical responses to subsolidus alteration of granitic rocks by oxidizing As-bearing fluids: REE arsenates and As-rich silicates from the Zinnwald granite, eastern Erzgebirge, Germany. *Canadian Mineralogist* 49, 913–930. https://doi.org/10.3749/canmin.49.4.913

Ginzburg A.L., Gorzhevskaya S.A., Sidorenko G.A. & Ukhina T.A. 1969: Wolframoixiolite – a variety of ixiolite. *Zapiski Vsesoyuznogo Mineralogicheskogo Obshchtstva* 98, 63– 73 (in Russian).

Hofmann M., Linnemann U., Gerdes A., Ullrich B. & Schauer M. 2009: Timing of dextral strike-slip processes and basement exhumation in the Elbe Zone (Saxo–Thuringian Zone): the final pulse of the Variscan Orogeny in the Bohemian Massif constrained by LA-SF-ICP-MS U–Pb zircon data. In: Murphy J.B. Keppie J.D. & Hynes A.J. (Eds.): Ancient Orogens and Modern Analogues. *Geological Society, London, Special Publications* 327, 197–214.

Hreus S., Výravský J., Cempírek J., Breiter K., Vašinová Galiová M., Krátký O., Šešulka V. & Škoda R. 2021: Scandium distribution in the world-class Li-Sn-W Cínovec greisen type deposit: Result of a complex magmatic to hydrothermal evolution, implications for scandium valorization. *Ore Geology Review* 139, 104433. https://doi.org/10.1016/j.oregeorev.2021.104433

Hulsbosch N. 2019: Nb–Ta–Sn–W distribution in granite-related ore systems: Fractionation mechanisms and examples from the Karagwe–Ankole Belt of Central Africa. In: Decreé S. & Robb L. (Eds.): Ore Deposits: Origin, Exploration, and Exploitation. *American Geophysical Union and John Wiley & Sons*, Hoboken, Washington D.C., 75–107. https://doi.org/10.1002/9781119290544.ch4

Johan V. & Johan Z. 1994: Accessory minerals of the Cínovec (Zinnwald) granite cupola, Czech Republic. Part 1: Nb-, Ta- and Ti-bearing oxides. *Mineralogy and Petrology* 51, 323–343. https://doi.org/10.1007/BF01159735

Krejčí Kotlanová M., Dolníček Z., René M., Prochaska W., Ulmanová J., Kapusta J., Mašek V. & Kropáč K. 2024: Fluid Evolution of Greisens from Krupka Sn-W Ore District, Bohemian Massif (Czech Republic). *Minerals* 14, 86. https://doi.org/10.3390/min14010086

Lahti S.I. 1987: Zoning in columbite-tantalite crystals from the granitic pegmatites of the Eräjärvi area, southern Finland. *Geochimica et Cosmochimica Acta* 51, 509–517. https://doi.org/10.1016/0016-7037(87)90065-2

Leopardi D., Gerdes A., Albert R., Gutzmer J., Lehmann B. & Burisch M. 2024a: LA-ICP-MS U–Pb cassiterite age data of the Sadisdorf deposit link Sn–Li–(W–Cu) mineralization in the eastern Erzgebirge to the collapse of the Altenberg–Teplice Caldera. *Geochemistry* 84, 126038. https://doi.org/10.1016/j.chemer.2023.126038

Leopardi D., Gutzmer J., Lehmann B. & Burisch 2024b: The Spatial and temporal evolution of the Sadisdorf Li–Sn–(W–Cu) magmatic–hydrothermal greisen and vein system, Eastern Erzgebirge, Germany. *Economic Geology* 119, 771–803. https://doi.org/10.5382/econgeo.5077

Linnen R.L. 1998: The solubility of Nb–Ta–Zr–Hf–Win granitic melts with Li and Li+F: constraints for mineralization in rare metal granites and pegmatites. *Economic Geology* 93, 1013–1025. https://doi.org/10.2113/gsecongeo.93.7.1013

Linnen R.L. & Keppler H. 1997: Columbite solubility in granitic melts: Consequences for the enrichment and fractionation of Nb and Ta in the Earth's crust. *Contributions to Mineralogy and Petrology* 128, 213–227. https://doi.org/10.1007/s004100050304

London D. 2008: Pegmatites. Mineralogical Association of Canada. *Canadian Mineralogist Special Publication* 10, 1–347. https://doi.org/10.2138/am.2009.546

Michaud J.A.-S. & Pichavant M. 2020: Magmatic fractionation and the magmatic–hydrothermal transition in rare metal granites: evidence from Argemela (Central Portugal). *Geochimica et Cosmochimica Acta* 289, 130–157. https://doi.org/10.1016/j.gca.2020.08.022

Mingram B. 1998: The Erzgebirge, Germany, a subducted part of northern Gondwana: geochemical evidence for repetition of early Palaeozoic metasedimentary sequences in metamorphic thrust units. *Geological Magazine* 135, 785–801. https://doi.org/10.1017/S0016756898001769

Möller P., Dulski P., Szacki W., Malow G. & Riedel 1988: Substitution of tin in cassiterite by tantalum, niobium, tungsten, iron and manganese. *Geochimica et Cosmochimica Acta* 52, 1497–1503. https://doi.org/10.1016/0016-7037(88)90220-7

Neiva A.M.R., Gomes C.L. & Silva P.B. 2015: Two generations of zoned crystals of columbite-group minerals from granitic aplite–pegmatite in the Gouveia area, central Portugal. *European Journal of Mineralogy* 27, 771–782. https://doi.org/10.1127/ejm/2015/0027-2473

Novák M., Černý P. & Uher P. 2003: Extreme variation and apparent reversal of Nb–Ta fractionation in columbite-group minerals from the Scheibengraben beryl–columbite granitic pegmatite, Maršíkov, Czech Republic. *European Journal of Mineralogy* 15, 565–574. https://doi.org/10.1127/0935-1221/2003/0015-0565

Pouchou J.L. & Pichoir F. 1985: "PAP" φ(ρZ) procedure for improved quantitative microanalysis. In: Armstrong J.T. (Ed.): Microbeam analysis. *San Francisco Press*, San Francisco, 104–106

Romer R.L. & Pichavant M. 2021: Rare metal (Sn, W, Ta–Nb, Li) granites and pegmatites. *Encyclopedia of Geology (Second Edition)*. Elsevier, Amsterdam, 840–846. https://doi.org/10.1016/B978-0-08-102908-4.00003-5

Rub A.K., Štemprok M. & Rub M.G. 1998: Tantalum mineralization in the apical part of the Cínovec (Zinnwald) granite stock. *Mineralogy and Petrology* 63, 199–222. https://doi.org/10.1007/BF01164151

Shannon R.D. 1976: Revised effective ionic radii and systematic studies of interatomic distances in halides and chalcogenides. *Acta Crystallographica* A32, 751–767.

Subramanian M.A., Aravamudan G. & Rao G.V.S. 1983: Oxide pyrochlores – a review. *Progress in Solid State Chemistry* 15, 55–143. https://doi.org/10.1016/0079- 6786(83)90001-8

Štemprok M., Holub F.V. & Novák J.K. 2003: Multiple magmatic pulses of the Eastern Volcano-Plutonic Complex, Krušné hory/Erzgebirge batholith, and their phosphorus contents. *Bulletin of Geosciences* 78, 277–296.

Taylor S.R. & McLennan S.M. 1985: The continental crust: Its composition and evolution. *Blackwell Scientific Publication*, Carlton, 1–312.

Tischendorf G., Gottesmann B., Förster H.-J. & Trumbull R.B. 1997: On Li-bearing micas: estimating Li from electron microprobe analyses and an improved diagram for graphical representation. *Mineralogical Magazine* 61, 809–834. https://doi.org/10.1180/minmag.1997.061.409.05

Uher P., Černý P., Chapman R., Határ J. & Miko O. 1998: Evolution of Nb–Ta oxide minerals in the Prašivá granitic pegmatites, Slovakia. II. External hydrothermal Pb,Sb overprint. *The Canadian Mineralogist* 36, 535–545.

Uher P., Malachovský P., Dianiška I. & Kubiš M. 2001: Rare-element Nb–Ta–W mineralization of the tin-bearing Spiš–Gemer granites, eastern Slovakia. *Geolines* 13, 119–120.

Van Lichtervelde M., Linnen R., Salvi S. & Beziat D. 2006: The role of metagabbro rafts on tantalum mineralization in the Tanco granitic pegmatite, Manitoba. *Canadian Mineralogist* 44, 625–644. https://doi.org/10.2113/gscanmin.44.3.625

Van Lichtervelde M.V., Holtz F. & Melcher F. 2018: The effect of disequilibrium crystallization on Nb–Ta fractionation in pegmatites: Constraints from crystallization experiments of tantalite–tapiolite. *American Mineralogist* 103, 1401–1416. https://doi.org/10.2138/am-2018-6441

Viladkar S.G. & Sorokhtina N.V. 2021: Evolution of pyrochlore in carbonatites of the Amba Dongar complex, India. *Mineralogical Magazine* 85, 554–567. https://doi.org/10.1180/mgm.2021.50

Warr L.N. 2021: IMA–CNMNC approved mineral symbols. *Mineralogical Magazine* 85, 291–320. https://doi.org/10.1180/mgm.2021.43

Wise M.A., Francis C.A. & Černý P. 2012: Compositional and structural variations in columbite-group minerals from granitic pegmatites of the Brunswick and Oxford fields, Maine: differential trends in F-poor and F-rich environments. *Canadian*

Mineralogist 50, 1515–1530. https://doi.org/10.3749/canmin.50.6.1515

Xie L., Wang R.C., Che X.D., Huang F.F., Erdmann S. & Zhang W.L. 2016: Tracking magmatic and hydrothermal Nb–Ta–W–Sn fractionation using mineral textures and composition: a case study from the late Cretaceous Jiepailing ore district in the Nanling Range in South China. *Ore Geology Reviews* 78, 300–321. https://doi.org/10.1016/j.oregeorev.2016.04.003

Zhang J., Liang X., Wang F., Wang H., Fan Y., Ba T. & Meng X. 2023: CorelKit: An Extensible CorelDraw VBA Program for Geoscience Drawing. *Journal of Earth Science* 34, 735–757. https://doi.org/10.1007/s12583-022-1772-4

Zhao Z., Yang X., Lu S., Lu Y., Sun Ch., Chen S., Zhang Z.Z., Bute S. I. & Zhao L. 2021: Genesis of Late Cretaceous granite and its related Nb–Ta–W mineralization in Shangbao, Nanling Range: Insights from geochemistry of whole-rock and Nb–Ta minerals. *Ore Geology Reviews* 131, 103975.